Brodogradnja Volume 77 Number 4 (2026) 77407

University of Zagreb
Faculty of Mechanical
Engineering and Naval
Architecture

journal homepage: www.brodogradnja.fsb.hr

Brodogradnja

An International Journal of Naval Architecture and
Ocean Engineering for Research and Development

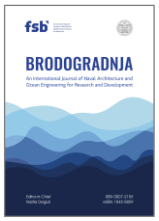

Assessment of parametric rolling using coupled numerical, CFD and experimental approaches

Anton Turk [1, *], *Zoran Čarija* [1], *Emre Uzunoglu* [2], *Jasna Prpić-Oršić* [1]

[1] *Faculty of Engineering, University of Rijeka, Croatia*
[2] *Centre for Marine Technology and Ocean Engineering (CENTEC), Instituto Superior Técnico, Universidade de Lisboa, Av. Rovisco Pais, 1049-001, Portugal*

ARTICLE INFO

Keywords:
Parametric rolling
CFD
Ship stability
Overset grids
Nonlinear roll motion
Wave–ship interaction

ABSTRACT

This study investigates parametric rolling of a container vessel in regular head waves using a hierarchical modelling framework combining a nonlinear time domain motion solver, a blended Ikeda-based roll damping module, and high-fidelity CFD simulations employing single-mesh and overset mesh strategies. The selected case corresponds to the classical resonance regime for first order parametric instability. All numerical approaches consistently reproduce the fundamental resonance mechanism, including the characteristic frequency relationship between pitch and roll and the exponential growth phase. A key result is the close agreement in instability onset time among the reduced order model and both CFD configurations, demonstrating robust capture of the excitation/restoring interaction governing parametric resonance. Experimental measurements exhibit an earlier visible onset, attributed to unavoidable perturbations and slight irregularities in the basin wave record, highlighting the sensitivity of parametric instability to initial disturbance levels. Differences in saturation amplitude are primarily associated with viscous dissipation modelling and nonlinear free surface phenomena, including green-water events observed experimentally but intentionally excluded from the present CFD setup. The results confirm that accurate representation of the resonance mechanism is achievable across modelling levels, while amplitude prediction remains sensitive to nonlinear damping and deck interaction effects. The developed framework provides a validated and computationally efficient basis for further investigations of damping thresholds, irregular wave excitation, green-water modelling, and coupled propulsion–roll interaction.

1. Introduction

Parametric rolling is one of the most critical nonlinear dynamic stability phenomena encountered by ships operating in longitudinal waves. It is characterized by large roll amplitudes induced by periodic variations of the ship's restoring moment, typically when the wave encounter frequency approaches twice the natural roll frequency. The phenomenon has been extensively documented through experimental and numerical investigations [1, 2] and has been formally addressed in stability criteria adopted by the

* Corresponding author.
E-mail address: anton.turk@riteh.uniri.hr

https://doi.org/10.21278/brod77407
Received 13 March 2026; Received in revised form 13 May 2026; Accepted 14 May 2026
Available online 21 May 2026
ISSN 0007-215X; eISSN 1845-5859

International Maritime Organization (IMO). Despite these efforts, reliable prediction of parametric rolling remains challenging due to strong nonlinearities, complex viscous damping mechanisms, and pronounced sensitivity to wave characteristics and disturbance levels. Parametric rolling can lead to extremely large roll angles, often developing suddenly and without direct wave excitation in the roll direction. Such motions pose a significant threat to ship safety, as they may result in loss of cargo, failure of lashing systems, and, in severe cases, capsizing. Several incidents involving large container vessels have demonstrated that parametric rolling can occur under relatively moderate sea states, making it a critical consideration in both ship design and operational guidance.

Traditional potential flow-based seakeeping methods are limited in their ability to represent nonlinear viscous effects, flow separation, vortex shedding, and appendage induced damping, all of which significantly influence roll response. [3, 4]. In addition, conventional frequency-domain formulations assume a fixed wetted hull surface and therefore cannot capture the nonlinear variation of the wetted area associated with large amplitude motions and free surface deformation. Because parametric rolling is inherently nonlinear, Computational Fluid Dynamics (CFD) has emerged as a powerful alternative capable of resolving the full viscous free surface flow field. Modern CFD approaches typically solve the Reynolds-Averaged Navier–Stokes (RANS) equations using the Finite Volume Method, enabling simultaneous representation of viscous effects, free surface deformation, and large rigid body motions. In particular, CFD inherently captures nonlinear roll damping mechanisms and allows direct modelling of appendages such as bilge keels and rudders.

Large amplitude roll motions introduce additional numerical challenges, particularly in relation to mesh deformation and grid quality. In mesh-deforming approaches based on the Arbitrary Lagrangian–Eulerian (ALE) formulation, the computational grid follows the motion of the body. While such morphing mesh techniques are efficient and widely used for small to moderate motions, large rotations and displacements can lead to severe cell distortion, loss of orthogonality, and degradation of numerical accuracy. In extreme cases, mesh tangling or negative cell volumes may occur, compromising solution stability and convergence. For this reason, ALE-based morphing mesh approaches are generally preferred for problems involving limited motion amplitudes, whereas alternative strategies are required for large-amplitude dynamics such as parametric rolling. Among available mesh motion strategies, the overset (chimera) technique has become widely adopted for parametric rolling simulations due to its ability to accommodate large rigid body motions without excessive mesh distortion, albeit at increased computational cost. The effectiveness of overset approaches has been demonstrated for various vessel types and wave conditions [5-7]. However, CFD simulations remain computationally demanding and require careful comparison against experimental data, which are limited in availability and often confined to specific benchmark configurations. The robustness and accuracy of overset mesh approaches in resolving complex hydrodynamic flows with large body motions have also been demonstrated in recent CFD studies [8].

Liu et al. [9] employed an unsteady RANS framework combined with dynamic overset grids to simulate parametric rolling of a KCS container ship in head seas, demonstrating good agreement with experimental measurements. Their results confirmed that CFD can accurately capture steady-state roll amplitudes, onset characteristics, and the influence of encounter frequency and initial roll angle. Several authors have further investigated the role of viscous damping and appendages using CFD. Yıldız et al. [10] and Kianejad et al. [4] demonstrated that CFD can provide improved estimation of amplitude dependent roll damping compared to empirical formulations. Wang et al. [11] and Zhang et al. [12] analyzed the KCS vessel under head wave conditions and confirmed that parametric rolling occurs when the encounter frequency approaches twice the natural roll frequency. More recently, Liu et al. [13] extended CFD investigations to full-scale simulations and examined scale effects, concluding that such effects have limited influence on the parametric roll mechanism itself. The coupling between parametric rolling and internal tank sloshing has also been explored, revealing significant modifications of the effective natural roll frequency and instability boundaries.

Recent research has also explored hybrid strategies, including machine learning assisted prediction of nonlinear ship responses [14, 15], as well as coupled multi-physics problems such as the interaction between parametric rolling and internal sloshing [16]. Nevertheless, systematic comparisons between reduced order

nonlinear models and high-fidelity CFD simulations under identical operating conditions remain scarce. In particular, the relative roles of viscous damping in governing instability onset versus saturation amplitude have not been clearly distinguished, and the sensitivity of instability triggering to experimental wave irregularities is often overlooked. Despite these advances, two main challenges remain. First, the computational cost of high-fidelity RANS simulations, especially when combined with dynamic overset meshes limits extensive parametric studies. Second, comparison opportunities are constrained by the limited availability of high-quality experimental datasets. Consequently, many CFD investigations focus on a restricted number of benchmark cases, most notably the KCS or C11 post-Panamax container ship under regular head waves. Recent studies have further demonstrated the applicability of CFD methods for analyzing nonlinear hydrodynamic phenomena relevant to ship stability and seakeeping. For example, Phuong et al. [17] performed a numerical investigation of scale effects on viscous roll damping for a container ship, highlighting the importance of viscous effects in accurately predicting roll behavior.

Additional CFD-based investigations have addressed related hydrodynamic problems, including the prediction of added resistance in waves [18] and wave-induced ship motions considering internal fluid dynamics such as tank sloshing [19], further demonstrating the versatility of CFD approaches in ship hydrodynamics research. Overall, the literature demonstrates that CFD methods, particularly unsteady RANS combined with VOF and dynamic mesh techniques, provide a robust framework for analyzing parametric rolling. They complement experimental investigations by offering detailed insight into viscous flow separation, vortex dynamics, free surface deformation, and appendage induced damping phenomena that are essential for understanding the nonlinear saturation and stability boundaries of parametric roll.

Despite the significant progress achieved in both experimental and numerical investigations of parametric rolling, several important gaps remain. Most existing studies either rely on reduced-order potential flow models with simplified damping formulations or employ high-fidelity CFD simulations without systematic comparison between different numerical strategies under identical conditions. In particular, the relative influence of mesh motion techniques, boundary treatment, and numerical dissipation on the prediction of instability onset and saturation amplitude has not been clearly established. Furthermore, the sensitivity of instability development to disturbance levels and wave irregularities is often overlooked in comparative studies.

The aim of the present study is to address these gaps by performing a consistent, multi-level analysis of parametric rolling using a nonlinear time-domain model, a semi-empirical damping formulation, and high-fidelity CFD simulations employing different mesh strategies. A key novelty of this work lies in the direct comparison of single-mesh and overset mesh CFD approaches under identical wave and operating conditions, without the introduction of artificial excitation, imposed asymmetry, or external perturbations. This allows the parametric instability to develop naturally from the governing physics, providing a clear assessment of the role of viscous effects, numerical dissipation, and modelling assumptions in the prediction of parametric rolling behaviour. This approach provides new insight into the robustness of instability prediction across modelling levels and establishes a consistent framework for evaluating nonlinear roll dynamics.

The objective of the present study is therefore to investigate parametric rolling under a classical resonance condition using a hierarchical modelling framework that combines a nonlinear time domain motion solver, a blended semi-empirical damping formulation, and CFD simulations employing both single-mesh and overset mesh strategies. By directly comparing these modelling levels with experimental measurements, the study aims to clarify the mechanisms governing instability onset and amplitude development, and to assess the extent to which viscous modelling influences the prediction of parametric roll.

2. Time domain nonlinear ship motion model

This section presents a time domain formulation of a coupled nonlinear ship motion model developed for the analysis of parametric rolling [1, 2]. The formulation of the nonlinear time-domain model is based on a set of simplifying assumptions consistent with conventional seakeeping theory. The fluid is assumed to be incompressible, inviscid, and irrotational, and surface tension effects are neglected. The ship is treated as a rigid body with six degrees of freedom, advancing at constant forward speed in regular waves in an open-

ocean environment. Hydrodynamic forces are evaluated based on potential flow assumptions, while nonlinear effects are introduced through time-varying hydrostatic restoring coefficients and instantaneous Froude–Krylov pressure integration. Viscous effects, which are not captured by potential flow theory, are represented separately using a semi-empirical nonlinear damping model.

The formulation is designed to retain the dominant nonlinear hydrodynamic mechanisms responsible for parametric resonance, while remaining computationally efficient for long duration simulations. The model follows a hybrid time–frequency concept, in which hydrodynamic coefficients are initially derived using linear potential flow theory, while the equations of motion are solved in the time domain with selected nonlinearities retained explicitly. This approach represents a compromise between fully nonlinear computational methods and traditional linear strip theory, providing sufficient accuracy for parametric rolling studies at a computational cost suitable for systematic investigations.

The present formulation may be classified as a 2.5D approach. While the hydrodynamic coefficients are obtained using conventional strip theory based on two-dimensional sectional analysis, the Froude–Krylov forces and restoring contributions are evaluated on the instantaneous wetted hull surface. This allows partial inclusion of three-dimensional and nonlinear geometric effects within an otherwise sectional framework.

In contrast to classical 2.5D strip theory methods, where Froude–Krylov forces are typically linearised and evaluated on the mean wetted surface, the present approach employs a body-exact evaluation of pressures, thereby improving the representation of time-varying hydrostatic and excitation effects. Such approaches are commonly referred to as 2.5D methods in the literature, as they bridge the gap between fully three-dimensional CFD simulations and simplified two-dimensional formulations [20].

2.1 General formulation

The ship is treated as a rigid body with six degrees of freedom, advancing at constant forward speed in regular longitudinal waves. The equations of motion are solved directly in the time domain, allowing large amplitude motions and time varying restoring characteristics to be resolved without linearization.

The governing equations of motion are expressed as:

$$\sum_{j=1}^{6}\left[\left(M_{kj}(t)+A_{kj}(\omega,t)\right)\ddot{\eta}_j+B_{kj}(\omega,t)\dot{\eta}_j+C_{kj}(t)\eta_j\right]=F_k^I(t);\quad \text{k=1, ..., 6} \tag{1}$$

where the subscripts k, j are associated with forces in the k -direction due to motions in the j-mode (k = 1, 2, 3 represent the surge, sway and heave directions, and 4, 5, 6 represent roll, pitch and yaw directions). M_{kj} are the components of the mass matrix for the ship, A_{kj} and B_{kj} are the added mass and damping coefficients, $C_{kj}(t)$ are the hydrostatic (time dependent) restoring coefficients, and F_k are the amplitudes of the exciting forces [1, 2].

The hydrodynamic coefficients used in the present formulation are obtained within the framework of strip theory Faltinsen [21] based on linear potential flow assumptions. Added mass and radiation damping coefficients are computed in the frequency domain for each transverse section of the hull and subsequently integrated along the ship length to obtain global coefficients. These calculations are performed for a range of encounter frequencies and forward speeds, and the resulting coefficients are introduced into the time-domain model through appropriate interpolation.

The restoring coefficients are evaluated using a nonlinear hydrostatic approach based on the instantaneous wetted hull geometry. In contrast to linear formulations, where restoring terms are derived from calm water conditions, the present model accounts for the variation of the righting arm due to wave-induced changes in the submerged geometry. This is achieved through direct computation of hydrostatic properties at each time step, allowing accurate representation of time-varying stability, which is essential for capturing parametric excitation.

Since viscous effects are not accounted for within potential flow theory, roll damping is introduced through a semi-empirical formulation. In the present study, damping is estimated using a modified Ikeda method, which accounts for the main physical components of roll damping, including frictional, wave-making, eddy-making, and lift contributions, as well as appendage effects.

2.2 Radiation forces and omission of hydrodynamic memory

Radiation forces are modelled using frequency dependent added mass and damping coefficients evaluated at the encounter frequency. In contrast to fully time domain potential flow formulations, hydrodynamic memory effects represented by convolution integrals (Cummins formulation) expressed as,

$$K(t-\tau)\dot{\eta}_j(\tau)d\tau \tag{2}$$

where $K(t)$ represents the memory kernel (impulse response function) are intentionally omitted.

In this work, radiation forces are instead represented by frequency dependent added mass and damping coefficients evaluated at the encounter frequency, without convolution in time. This assumption implies that the hydrodynamic force at a given instant depends only on the current state of motion and not explicitly on its history. The omission of memory effects is a deliberate and justified simplification. For the low encounter frequencies typically associated with parametric rolling in longitudinal seas, the contribution of radiation damping to the overall roll response is relatively small compared to hydrostatic restoring variation and viscous damping. Furthermore, for large amplitude roll motions, viscous effects dominate the energy dissipation mechanism, reducing the practical significance of radiation memory terms. This modelling choice reflects the physics of parametric rolling, where nonlinear restoring variation and viscous damping dominate the roll response, particularly once large amplitude motions develop. Neglecting memory effects reduces computational complexity while preserving the dominant mechanisms governing parametric instability.

2.3 Two and a half dimensional Froude–Krylov formulation

A feature of the present approach is the adoption of 2.5D Froude–Krylov force formulation based on the incident wave pressure field [1, 20, 22]). The instantaneous incident wave pressure is evaluated using the full three-dimensional wave elevation along the ship length, while force and moment integration is performed on a strip-wise basis. At each time step, the instantaneous wetted surface of the hull is determined by intersecting the ship geometry with the incident wave profile. The corresponding pressure distribution is then integrated over the wetted surface to obtain nonlinear restoring moments. This procedure is essential for capturing the parametric variation of righting arm characteristics that drives parametric resonance.

The local incident pressure is given by:

$$p_{FK}(\boldsymbol{x},t) = \rho g[\eta(x,t) - z] \tag{3}$$

where $\boldsymbol{x} = (x,y,z)$ denotes spatial coordinates on the instantaneous wetted hull surface, ρ is the fluid density, g is gravitational acceleration, $\eta(x,t)$ is the incident wave elevation along the ship length, and z is the vertical coordinate of the surface element measured from the still water level. For each transverse strip i, the corresponding force and moment contributions are calculated as

$$F_{FK} = \iint_{Si} p_{FK}(\boldsymbol{x},t)n\, dS \tag{4}$$

$$M_{FK} = \iint_{Si} r \times p_{FK}(\boldsymbol{x},t)n\, dS \tag{5}$$

where r is the position vector from the chosen reference point (typically the center of gravity) to the surface element. The nonlinear hydrostatic contribution is therefore treated quasi-statically, reflecting the immediate dependence of restoring forces on the vessel's instantaneous displacement relative to the free surface where the restoring variation plays a dominant role compared to radiation effects. This hybrid formulation preserves the longitudinal variation of the wave field that governs parametric excitation, while maintaining numerical efficiency comparable to classical strip methods.

2.4 Numerical solution procedure

At each time step, the instantaneous ship position and orientation are updated, and the wetted geometry of each strip is recalculated based on the current wave elevation. Nonlinear hydrostatic and Froude–Krylov forces are then integrated and combined with radiation and damping terms. The equations of motion are advanced using an explicit time integration scheme, allowing stable simulation of long-time histories required for parametric rolling analysis.

The adopted time domain formulation is specifically tailored to investigate parametric rolling phenomena in head and near-head seas. The driving mechanism of parametric rolling, periodic variation of restoring stiffness at approximately twice the natural roll frequency, is inherently nonlinear and cannot be captured by linear frequency domain methods alone.

By allowing restoring coefficients to vary with instantaneous wave elevation and ship motion, the present model reproduces the essential physics of parametric excitation. At the same time, the simplified treatment of radiation forces and the omission of memory effects make long simulations feasible, enabling systematic exploration of stability boundaries and roll amplitude growth.

The model therefore provides a robust numerical platform for comparing experimental observations, semi-empirical damping models, and newly introduced CFD-based damping corrections, which form the novel contribution of the present study.

3. Nonlinear roll damping model and its relation to CFD analysis

As mentioned in previous section the nonlinear equations of motion are solved using an explicit time-integration scheme. At each time step, the following sequence is performed:

1. The instantaneous ship position and orientation are updated.
2. The wetted geometry of each transverse strip is recalculated based on the incident wave elevation.
3. Hydrostatic and Froude–Krylov pressures are integrated to obtain nonlinear restoring forces and moments.
4. Hydrodynamic radiation and diffraction forces are evaluated using precomputed frequency domain coefficients.
5. Damping forces are applied using the nonlinear damping model described in this Section 3.
6. Accelerations are computed from the equations of motion and integrated to advance velocities and displacements.

3.1 Role of damping in parametric rolling

Roll damping is a governing factor in the development, growth, and saturation of parametric rolling motions. Unlike linear roll response problems, where damping may be represented adequately using linear frequency dependent coefficients, parametric rolling is characterised by strongly nonlinear energy exchange mechanisms. Once parametric resonance is initiated, roll amplitudes may increase rapidly until nonlinear dissipative effects counterbalance the excitation.

Accurate modelling of roll damping is therefore essential for reliable prediction of parametric rolling. A lower value estimate may lead to unrealistically large roll amplitudes, while excessive damping may artificially suppress instability that would otherwise develop under given wave conditions.

3.2 Limitations of potential flow based damping formulations

In classical potential flow theory, roll damping is primarily associated with radiated wave energy. Such formulations inherently assume inviscid and irrotational flow and therefore neglect viscous effects. While this assumption may be acceptable for small amplitude oscillatory motions, it becomes increasingly invalid as roll amplitudes grow. Parametric rolling is typically accompanied by large roll angles, flow separation at the bilges, formation of strong vortical structures, and viscous dissipation in the vicinity of the free surface. These phenomena constitute dominant damping mechanisms and cannot be captured by potential flow-based approaches, even when nonlinear restoring effects are partially introduced. As a consequence, potential flow methods tend to underestimate roll damping in the nonlinear regime, leading to overprediction of roll amplitudes and incorrect estimation of instability saturation behaviour. This fundamental limitation motivates the introduction of nonlinear damping representations within time domain models.

3.3 Semi-empirical nonlinear roll damping formulation

To overcome the above limitations, roll damping in the present model is introduced using a nonlinear, velocity dependent formulation. The damping moment is expressed as a combination of linear and higher order terms:

$$B_{44}(\dot{\eta}_4) = B_{44,1}\dot{\eta}_4 + B_{44,2}\dot{\eta}_4\left|\dot{\eta}_4\right| + B_{44,3}\dot{\eta}_4^{\,3} \tag{6}$$

in which the first term is linear, the second term represents quadratic drag, and the third term is cubic denoted through roll angular velocity, with damping coefficients determined through experimental data and numerical calibration. This formulation allows the dissipative forces to increase nonlinearly with roll velocity, reflecting the physical mechanisms of viscous energy dissipation caused by vortex shedding, flow separation, and free surface effects. Such behaviour is essential for realistic prediction of roll amplitude saturation under parametric excitation. The equivalent coefficient of roll damping components is expressed in terms of its various contributions [23]. The total damping coefficient is obtained from,

$$B_e = B_F + B_E + B_W + B_L + B_{BK} \tag{7}$$

in which the component damping coefficients are as follows: B_F equals hull skin friction damping, B_E equals hull eddy shedding damping, B_W equals free surface wave damping, B_L equals lift force damping, and B_{BK} equals bilge keel damping. It is a component discrete type prediction method which was developed by Ikeda et al and coded separately from time domain solver.

3.4 Coupling of the damping model with the time domain solver

The nonlinear roll damping model is fully integrated into the time domain equations of motion described in Section 2. At each time step, the instantaneous roll velocity is evaluated, and the corresponding damping moment is applied directly within the governing equations. This explicit coupling ensures that damping evolves dynamically as roll amplitudes increase. Unlike linear damping formulations, the present approach remains valid throughout the nonlinear response regime and enables physically consistent simulation of both the growth and saturation phases of parametric rolling.

3.5 Relation to CFD based damping assessment

Although the nonlinear damping model represents a substantial improvement over potential flow-based approaches, its parameters remain semi-empirical in nature. To further enhance physical realism and reduce reliance on empirical tuning, high-fidelity CFD simulations are introduced as a complementary analysis tool. CFD simulations inherently resolve viscous flow phenomena, including vortex shedding, flow separation at the bilges, and appendage induced effects. These mechanisms play a crucial role in roll damping at large amplitudes and are directly accessible through CFD predicted hydrodynamic moments. By analysing CFD results during large amplitude roll motions, effective damping characteristics can be extracted and compared with the assumed nonlinear damping formulation. This comparison enables assessment of the validity and limitations of the reduced order damping model under various operating conditions.

3.6 Motivation for CFD augmentation

The primary motivation for introducing CFD within the present framework is not to replace the nonlinear parametric resonance model, but to complement and strengthen it. CFD provides detailed insight into flow-induced damping mechanisms, while the time domain model remains computationally efficient and suitable for systematic parametric studies. The combined use of experimental data, nonlinear time domain modelling,

and CFD based analysis establishes a comprehensive and physically consistent framework for the assessment of parametric rolling in container ships.

4. Emphasis on convergence between time domain and damping models

As stated, nonlinear roll damping module was developed separately based on the latest formulation of the Ikeda method. Acknowledging the semi-empirical nature and known limitations of the original Ikeda approach under strongly nonlinear parametric rolling conditions, a blending strategy was introduced to improve robustness and extend applicability to large roll amplitudes. A key aspect of the proposed numerical framework is the iterative coupling and convergence between the time domain motion solver and the nonlinear damping model, which together enable the simulation of strongly nonlinear roll dynamics associated with parametric resonance. Rather than prescribing damping coefficients a priori, the damping forces are evaluated dynamically based on the instantaneous roll motion and subsequently fed back into the time domain equations of motion. This creates a closed-loop numerical procedure in which ship motions and hydrodynamic damping mutually influence each other with computational workflow seen in Figure 1.

In each simulation step, the time domain model provides the current state variables—roll angle, angular velocity, and acceleration, which are then used to evaluate the corresponding damping forces within the dedicated damping module. These forces account for nonlinear effects arising from viscous flow separation, vortex shedding, and appendage induced losses. The updated damping forces are reintroduced into the time domain solver, and the solution is iterated until convergence is achieved within a prescribed tolerance. This converged interaction between motion prediction and damping evaluation allows the nonlinear behaviour to emerge naturally from the numerical scheme, rather than being enforced through empirical linearization.

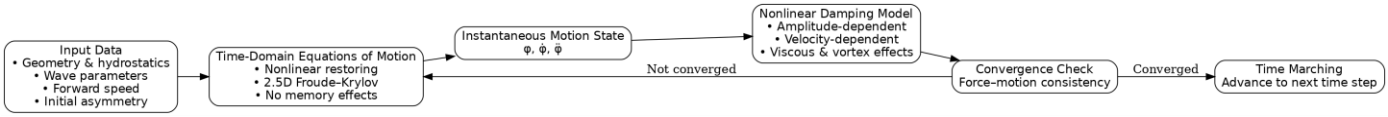

Fig. 1 Computational workflow of the time domain parametric roll model

Steps 2–4 are repeated iteratively within the same time step until convergence is achieved based on motion and force residuals. This approach is fundamentally different from conventional potential flow-based time domain models relying on the Cummins equation and associated memory effects. In the present methodology, radiation forces are not modelled via convolution integrals, and no assumption is made regarding linear frequency dependent damping. Instead, the nonlinear damping contribution is treated explicitly in the time domain, avoiding the inherent limitations of memory-based formulations when applied to large amplitude roll motions. This choice is particularly justified for parametric rolling, where the dominant dissipative mechanisms are highly nonlinear and cannot be adequately represented through linear radiation damping.

The convergence between the time domain solver and the damping model plays a crucial role in accurately capturing the saturation of roll amplitudes observed in parametric rolling events. While potential flow methods are capable of predicting the onset of instability, they generally fail to reproduce the post-critical steady state behaviour due to inadequate damping representation. In contrast, the present coupled approach demonstrates that the balance between parametric excitation and nonlinear dissipation can be resolved numerically through iterative convergence, leading to physically realistic roll amplitudes without resorting to artificial damping corrections. By enforcing consistency between motion response and damping estimation at each time step, the proposed framework effectively embeds nonlinearity into the governing equations. This makes the model particularly suitable for studying sensitivity to wave parameters, ship loading conditions, and damping characteristics, and provides a robust basis for later comparison with CFD results. The methodology thus serves as an intermediate but essential link between simplified potential models and fully resolved CFD simulations.

5. CFD computational method

The CFD simulations are performed under a different set of assumptions compared to the potential-flow formulation presented in Section 2. The fluid is assumed to be viscous, incompressible, and Newtonian, and the flow is governed by the Reynolds-Averaged Navier–Stokes (RANS) equations. Turbulence effects are modelled using an appropriate closure model.

The free surface is captured using a Volume of Fluid (VOF) approach, allowing direct simulation of wave propagation, breaking, and deck overtopping. The ship is treated as a rigid body with six degrees of freedom, and its motion is resolved through dynamic coupling with the flow solver. The computational domain represents an open-water environment, with appropriate boundary conditions applied to minimise wave reflection and ensure stable wave generation. In contrast to the potential-flow assumptions adopted in Section 2, the CFD model accounts for viscous effects, turbulence, and fully nonlinear free-surface interactions. The numerical setup follows established best practices for ship hydrodynamics CFD simulations, in accordance with the ITTC Recommended Procedures and Guidelines for CFD applications [24].

5.1 Governing equations

The fluid was treated as incompressible and viscous. The flow field was described by the unsteady Reynolds-Averaged Navier–Stokes (URANS) equations:

$$\frac{\partial \rho}{\partial t} + \frac{\partial}{\partial t}(\rho \cdot u_i) = 0 \tag{8}$$

$$\frac{\partial}{\partial t}(\rho u_i) + \frac{\partial}{\partial x_j}(\rho u_i u_j) = -\frac{\partial p}{\partial x_i} + \frac{\partial}{\partial x_j}\left[\mu\left(\frac{\partial u_i}{\partial x_j} + \frac{\partial u_j}{\partial x_i} - \frac{2}{3}\delta_{ij}\frac{\partial u_l}{\partial x_l}\right)\right] + \frac{\partial}{\partial x_j}\left(-\rho\overline{u_i' u_j'}\right)_i \tag{9}$$

The Reynolds stress term $(-\rho\overline{u_i' u_j'})$ is related to the mean velocity gradients by the Boussinesq hypothesis as:

$$-\rho\overline{u_i' u_j'} = \mu_t\left(\frac{\partial u_i}{\partial x_j} + \frac{\partial u_j}{\partial x_i}\right) - \frac{2}{3}\left(\rho k + \mu_t \frac{\partial u_i}{\partial x_i}\right)\delta_{ij} \tag{10}$$

where u are the velocity components and ρ, p, μ, are the fluid density, the pressure, dynamic viscosity to obtain body force and viscosity stress, respectively.

5.2 Turbulence model

Turbulence closure was achieved using the SST k−ω model originally proposed by Menter [25]. The model combines the near-wall accuracy of the k−ω formulation with the free stream robustness of the k−ε model through blending functions. It also incorporates a shear/stress limiter that improves prediction of separation under adverse pressure gradients. For simulations involving parametric rolling, where large roll amplitudes induce strong bilge separation and dynamically varying boundary layers, the SST model provides improved prediction of viscous damping compared to the standard k−ε formulation. It was therefore selected for all simulations.

5.3 Free surface modelling

The air–water interface was captured using the Volume-of-Fluid (VOF) method originally introduced by Hirt and Nichols. An additional scalar transport equation for the liquid volume fraction α was solved:

$$\frac{\partial \alpha}{\partial t} + \nabla(\alpha \cdot \mathrm{u}) = 0 \tag{11}$$

Local fluid properties were evaluated as volume-fraction-weighted averages of the two phases. The convective term in the volume fraction equation was discretised using a second order High-Resolution Interface Capturing (HRIC) scheme [26] to maintain a sharp interface. With appropriate mesh refinement, the interface thickness remained confined to one to two cells. The VOF and SST models are coupled through the RANS equations, allowing simultaneous resolution of nonlinear wave–body interaction and viscous damping mechanisms.

5.4 Numerical discretisation and solution strategy

The governing equations were discretised using the finite volume method on arbitrary polyhedral control volumes. The numerical solution is obtained using the implicit unsteady segregated solver available in Siemens STAR-CCM+. The governing equations are solved using an Algebraic Multigrid (AMG) linear solver with a Gauss–Seidel relaxation scheme. Flexible multigrid cycles are applied for the velocity and turbulence equations, while F-cycles are used for pressure and V-cycles for the volume fraction equation. Within each time step, the solution is advanced through a series of inner iterations. Each iteration consists of solving the momentum equations, the pressure-correction equation using the SIMPLE algorithm, and the transport equations for turbulence quantities and volume fraction. A total of 10 inner iterations are performed per time step to ensure adequate convergence of the coupled flow variables.

The time step is selected to maintain a Courant number below unity throughout the computational domain, ensuring numerical stability and accurate resolution of the free-surface flow. Under-relaxation factors of 0.4 for pressure and 0.7 for all other variables are applied to promote stable convergence of the iterative solution procedure. This approach provides stable and accurate resolution of transient free-surface flows and is widely used for URANS–VOF simulations. The use of inner iterations within each time step effectively ensures sufficient pressure–velocity coupling, analogous to multi-correction approaches employed in other CFD frameworks [27].

A time-step sensitivity study was conducted using Δt = 0.01, 0.005, and 0.0025 s, ($\Delta t/2$ and $\Delta t/4$). Simulations were restarted from an identical flow field at t = 1070 s and continued for an additional 80 s, corresponding to approximately 7.5 wave periods. The results in Figure 2 show negligible differences in both roll and pitch responses, indicating that the solution is effectively independent of time-step size within this range.

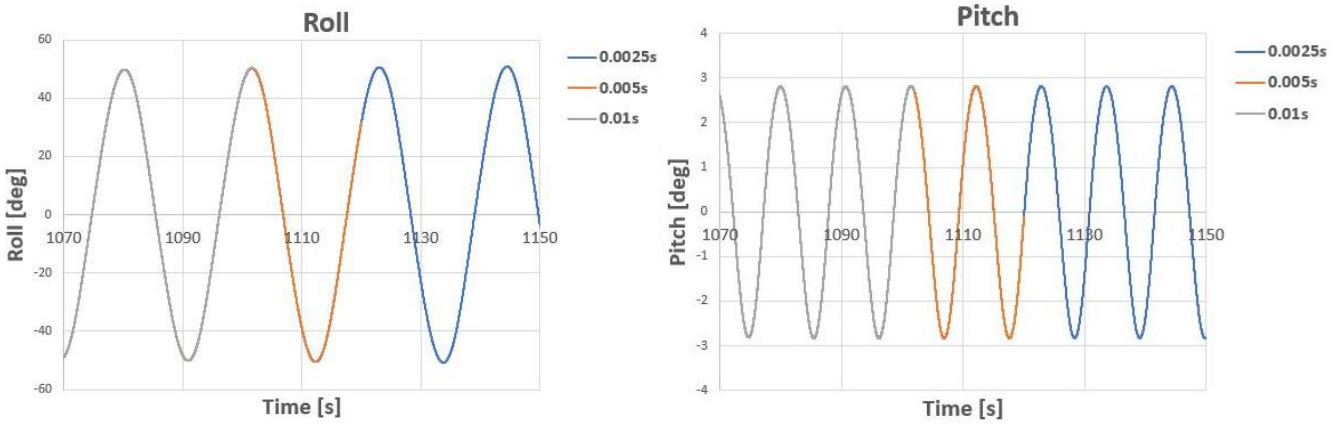

Fig. 2 Time sensitivity study for roll and pitch responses

The time step was selected following STAR-CCM+ guidelines for wave modelling, where the time step is initially estimated based on the wave period and spatial resolution. This value was further reduced to ensure that the Courant number remained below unity (with values in the majority of the domain significantly below 0.5) throughout the computational domain. The final selected time step is Δt = 0.01 s, which ensures numerical stability and accurate resolution of the free-surface flow.

Furthermore, using a fixed time step of Δt = 0.01 s, for the selected test condition, the wave period is T_w = 12.95 s, while the corresponding encounter period at U = 8 kn in head waves is approximately T_e =10.8 s. The adopted time step therefore corresponds to approximately 1080 time steps per encounter period, ensuring adequate temporal resolution of both wave excitation and ship response.

5.5 Computational domain and mesh strategy

Two numerical configurations were employed in order to assess the influence of mesh motion strategy and far field treatment on the prediction of parametric rolling. Naming of the domain external boundaries is

visible in Figure 3, while implemented boundary conditions in the CFD numerical model can be seen in Table 1.

Table 1 Boundary conditions

Domain name	Boundary condition	Velocity	Phase
INLET	Velocity inlet	Wave + v_{ship}	Water; bellow FS Air; above FS
OUTLET	Velocity inlet	Wave + v_{ship}	Water; bellow FS Air; above FS
RIGHT SIDE	Velocity inlet	Wave + v_{ship}	Water; bellow FS Air; above FS
LEFT SIDE	Velocity inlet	Wave + v_{ship}	Water; bellow FS Air; above FS
TOP	Pressure outlet	Calculated	Air
BOTTOM	Velocity inlet	Wave + v_{ship}	Water

5.5.1 Single-mesh domain configuration

In the first configuration, a single-mesh (no overset) was used, where grid movement is directly related to the calculated rigid body motion of the ship. Wave generation and absorption were achieved using forcing zones applied along the vertical boundaries of the computational domain. Within these zones, the Navier–Stokes solution was gradually blended towards a prescribed potential flow wave solution. This approach ensures stable wave propagation and minimises spurious reflections while maintaining a fully viscous solution in the vicinity of the ship.

The upstream boundary was prescribed as a velocity inlet with a fifth order Stokes wave superimposed with the forward ship speed. The top boundary was defined as a pressure outlet. While computationally efficient, the single-mesh approach may introduce mesh distortion under large amplitude roll motions, potentially affecting numerical dissipation and solution robustness.

5.5.2 Overset (chimera) mesh configuration

In the second configuration, an overset (chimera) grid technique was employed to improve mesh quality during large rigid body motions. The overset (chimera) mesh employs a cell-based interpolation scheme to transfer solution variables between overlapping grids. The interpolation is performed using a conservative approach to ensure continuity and stability of the flow field across mesh interfaces. The ship was enclosed within a body-fitted moving mesh block, which overlaps with a stationary background grid. Interpolation between the overlapping regions ensures continuous solution transfer during motion. A linear interpolation scheme based on shape functions is employed in all overset simulations, ensuring accurate and stable data exchange between overlapping meshes. Forcing zone with the defined length of influence were defined on all domain vertical boundaries (Inlet, Outlet, Left Side, Right Side). With this forcing approach a theoretical wave solution is applied at the zone near boundaries of a computational domain.

To minimise artificial wave reflection and maintain solution stability, forcing zones were defined at a distance of 0.4 *Lpp* from the lateral and upstream boundaries, and 1.0 *Lpp* upstream of the ship. This arrangement confines the fully resolved Navier–Stokes solution to the near field region, while gradually enforcing the target potential flow wave solution away from the ship. The overset approach eliminates large mesh movement of the background grid during large roll angles and allows more consistent resolution of viscous flow separation and bilge vortex formation. This configuration, although computationally more demanding, provides improved robustness for severe parametric roll simulations.

While overset mesh techniques are widely recognized for their robustness in handling large-amplitude motions, the objective of the present study is not to identify a single optimal approach, but rather to assess the influence of different numerical strategies on the prediction of parametric rolling. For this reason, both single-mesh and overset configurations are considered, allowing a systematic comparison under identical conditions.

5.5.3 Computational domain and mesh resolution

The numerical mesh was generated using a trimmed cell approach applied to the previously constructed ship geometry. The vessel was positioned centrally within a rectangular computational domain whose dimensions were defined relative to the ship length between perpendiculars (*Lpp*). The domain extended 1.0 *Lpp* upstream of the bow, 1.6 *Lpp* downstream of the stern, 1.5 *Lpp* below the keel, 1.2 *Lpp* laterally on both sides, and 0.8 *Lpp* above the calm water level. This configuration ensures sufficient distance between the ship and the outer boundaries to minimise reflection and boundary induced disturbances. A representation of the computational domain is shown in Figure 3.

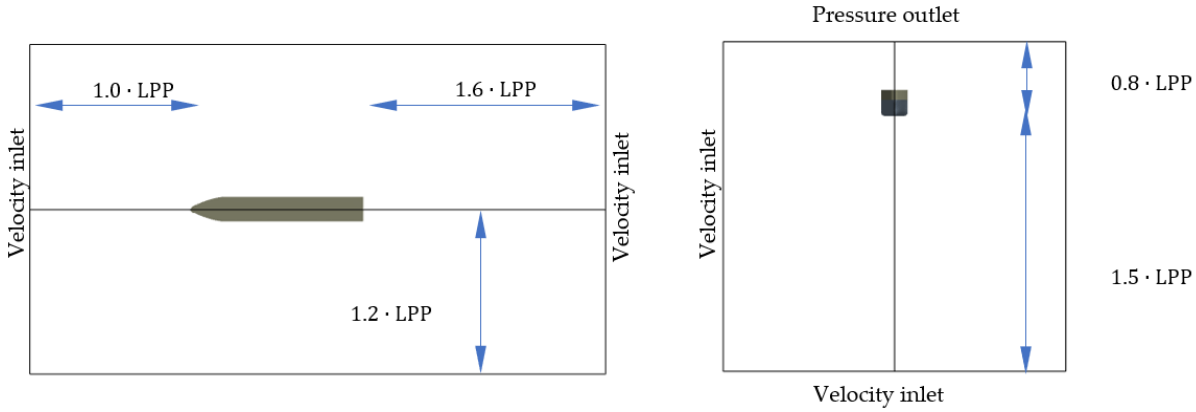

Fig. 3 Representation of the computational domain

Special attention was devoted to mesh refinement in regions where high gradients of velocity, pressure and free surface elevation were expected. Local refinement was introduced in the vicinity of the hull, within the free surface zone, and in the wake region. In order to properly capture wave kinematics, the mesh resolution in the longitudinal direction provided approximately 100 cells per wavelength, while the vertical discretisation near the free surface ensured approximately 22 cells per wave height. This level of discretization is consistent with established practices in CFD simulations of free-surface flows. Previous studies have employed resolutions of approximately 15 cells per wave height, while higher-fidelity simulations may use up to 30 cells. The present resolution therefore lies within the recommended range and ensures accurate representation of the wave field and associated hydrodynamic response. This is consistent with recent studies [28, 29], where similar or slightly lower resolutions are employed to accurately capture wave elevation and hydrodynamic interactions. Such resolution was found necessary for accurate representation of nonlinear wave deformation during large roll motions. To resolve the turbulent boundary layer, six prism layers were generated on the hull surface using 1.6 prism layer starching factor. The simulations were performed using a standard wall functions approach achieving an average dimensionless wall distance of $y^+ \approx 2000$, which is consistent with high Reynolds number full-scale ship simulations. The adopted wall treatment is appropriate for global force prediction and large amplitude motion assessment, while maintaining computational feasibility for long unsteady simulations.

5.6 Mesh sensitivity study for parametric rolling

Three mesh densities (M1–M3) listed in Table 2 were investigated to assess grid dependence with an example of M1 in Figure 4.

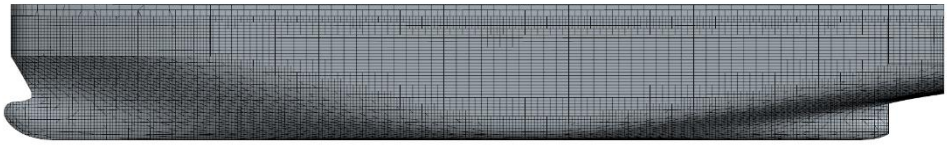

Fig. 4 Numerical mesh on ship surface, left (port) side view (Mesh M1)

The initial mesh selection was based on calm water simulations allowing two degrees of freedom (heave and trim). Ship resistance, trim and sinkage were used as quantitative indicators of solution convergence. Ship resistance was selected as the primary mesh quality metric due to its sensitivity to pressure distribution and viscous effects, and because it provides a clear asymptotic trend with mesh refinement.

The baseline mesh design was initially established through calm-water resistance simulations at a forward speed of 8 knots. This preliminary study allowed identification of regions requiring enhanced resolution, particularly in the vicinity of the free surface and along the hull.

Based on this analysis, local mesh refinement was introduced and extended vertically to account for large-amplitude motions and the potential submergence of the hull sides during parametric rolling.

The adequacy of the resulting mesh was subsequently verified under wave conditions through a dedicated mesh sensitivity study (M1–M3), performed for fully developed parametric rolling. The results demonstrate that the selected mesh (M2) provides a consistent prediction of roll and pitch responses, confirming that the adopted resolution is sufficient for the present analysis.

The results demonstrated that resistance converges asymptotically with increasing mesh density as seen in Figure 5. The medium density mesh (M2), consisting of approximately 1.5 million cells, provided a satisfactory compromise between accuracy and computational cost, and was selected for all subsequent calculations providing adequate resolution of wave propagation and nonlinear motion coupling. Additional verification was performed by evaluating roll response under wave conditions, confirming that further refinement produced negligible changes in predicted roll amplitude and frequency characteristics.

Table 2 Influence of ship resistance on numerical mesh size

Mesh name	Mesh size	Cells per wave length	Cells per wave height	Cell size dX	Cell size dZ	Fx	Trim	Heave
[-]	**10^6 [cells]*	*[-]*	*[-]*	*[m]*	*[m]*	*[kN]*	*[°]*	*[m]*
M1	0,52	66	16	3,9	0,49	992	0,0600	-0,240
M2	1,46	100	22	2,6	0,32	795	0,0635	-0,443
M3	3,98	150	36	1,5	0,21	782	0,0638	-0,460

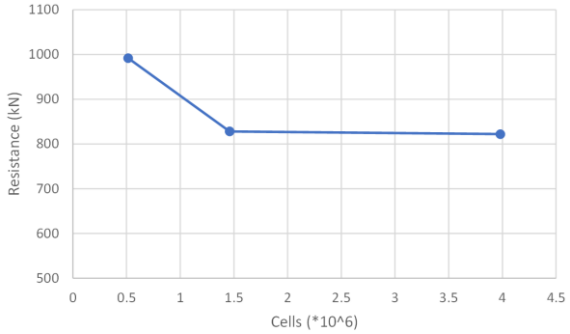

Fig. 5 Mesh convergence study based on ship resistance

Roll decay tests are commonly used in the literature for the verification of roll damping models [30-32]. However, such tests primarily address damping characteristics in calm water and do not capture the strongly nonlinear, wave-induced mechanisms governing parametric rolling.

In the present study, the mesh sensitivity analysis is therefore performed directly on fully developed parametric rolling, which represents the physical phenomenon of interest. A mesh sensitivity analysis was further tested using three grid resolutions (M1, M2, and M3) under conditions representative of fully developed parametric rolling. All simulations were carried out using the same time step ($\Delta t = 0.01$ s), starting from an identical flow field at $t = 1070$ s and continued for an additional 80 s (approximately 7.5 wave periods).

The comparison of roll and pitch responses in Figure 6 indicates that the results obtained with meshes M2 and M3 are nearly identical, while the coarsest mesh (M1) shows a small deviation in roll amplitude of approximately 0.7°. The pitch response is nearly identical across all meshes, as it is primarily governed by the incoming wave field.

These results confirm that mesh M2 provides a sufficient level of accuracy while maintaining reasonable computational cost, and it is therefore adopted for the simulations presented in this study.

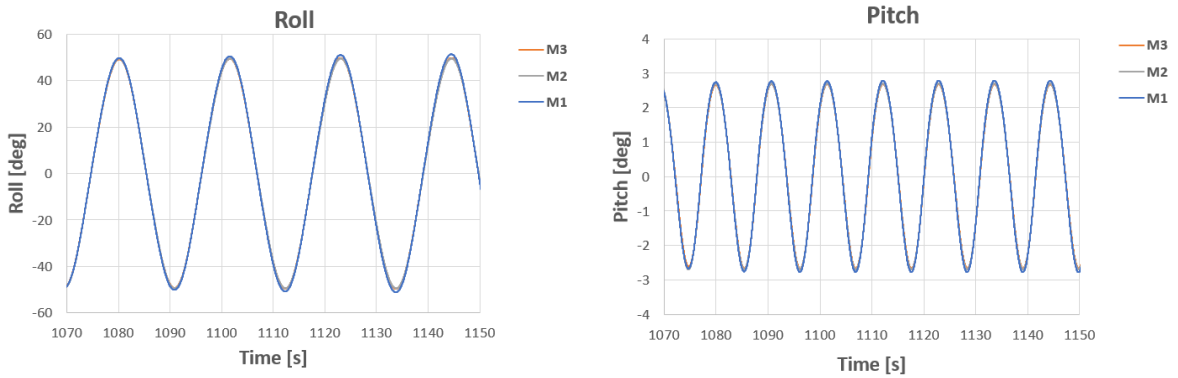

Fig. 6 Mesh convergence study based on calculated roll and pitch

5.7 Near-wall treatment and y⁺ distribution

At the high Reynolds numbers characteristic of full-scale conditions, as considered in the present study, the boundary layer along the hull is relatively thick and the logarithmic region of the velocity profile extends to significantly larger distances from the wall compared to model-scale conditions. This justifies the use of wall-function approaches in combination with relatively high y values.

To assess the distribution of y^+, a statistical analysis was performed over the wetted hull surface. The results, presented in terms of surface-area fraction, indicate that y^+ is not uniform, but exhibits a well-defined distribution with dominant values concentrated around the target range. This confirms that the wall-function treatment is applied consistently over the hull surface.

In order to evaluate the influence of near-wall resolution on the predicted response, additional simulations were performed using identical grids with varying prism-layer thicknesses applied on M2, resulting in average values of $y^+ \approx 1100$, 2000, and 2700. The resulting roll and pitch responses for the three cases are presented in Figure 7, showing a very close agreement between the solutions.

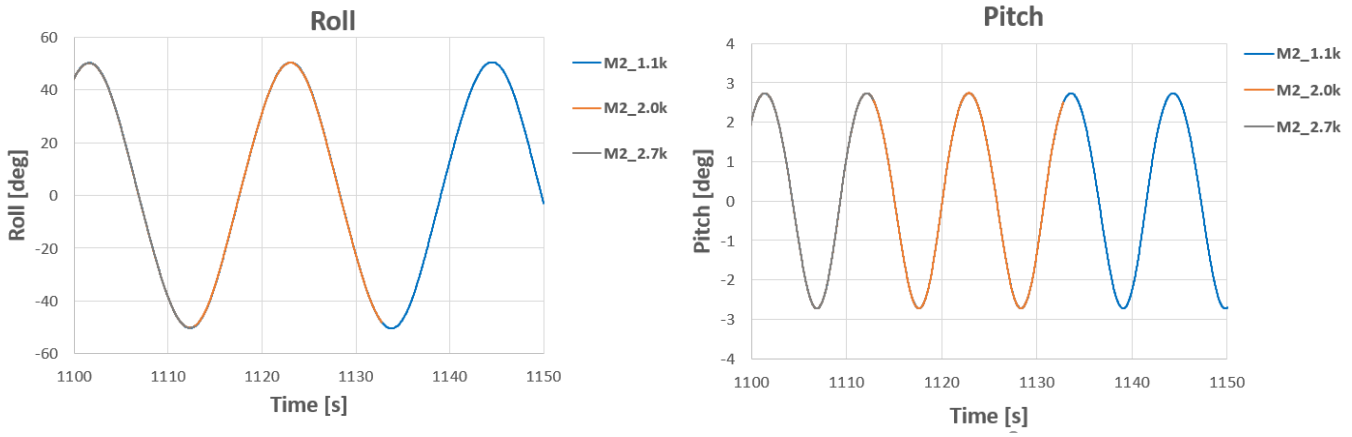

Fig. 7 Effect of Near-wall resolution (y^+) on predicted roll response

The comparison of the resulting roll responses shows very good agreement between all cases, with differences in extreme roll amplitudes of approximately 0.1°. This indicates that the global parametric rolling behaviour is not significantly affected by the near-wall resolution. In addition, the distribution of y^+ over the wetted hull surface, expressed as a fraction of total area, is shown in Figure 8, illustrating the spatial variation and dominant range of y^+ values for the analysed configurations. The adopted y^+ range ensures appropriate resolution of the logarithmic region of the turbulent boundary layer required for the application of standard wall functions, while simultaneously reducing the risk of numerical ventilation effects that may occur in excessively refined near-wall meshes during violent free-surface simulations [33, 34]. Nevertheless, it should be acknowledged that the adopted approach does not constitute a fully wall-resolved simulation and therefore cannot capture viscous sublayer flow structures.

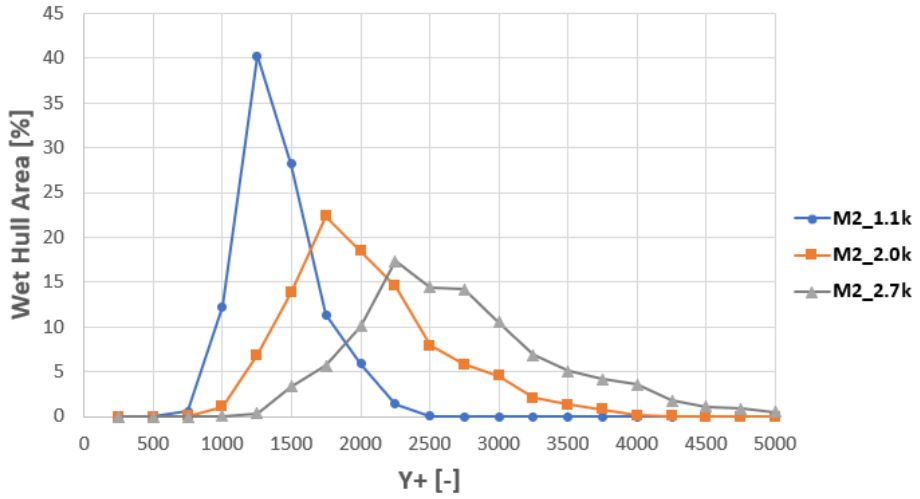

Fig. 8 Distribution of y^+ over the wetted hull surface expressed as a fraction of total area

These findings confirm that the adopted wall-function approach is appropriate for the present simulations and that the observed dissipation and saturation behaviour are not primarily numerical artefacts associated with near-wall modelling.

6. Results

The results presented in this section are derived from a multilevel modelling strategy combining a nonlinear time domain motion solver, an independently formulated roll damping module based on the latest Ikeda methodology, and high-fidelity CFD simulations. The motion solver and the damping module were developed separately in Fortran, while their interaction was realized through a C++ coupling interface enabling iterative exchange of kinematic states and nonlinear damping forces at each time step. This architecture

ensured numerical consistency while allowing controlled assessment of viscous dissipation effects on the instability growth and saturation phases.

The damping formulation relies on a blended implementation of the contemporary Ikeda approach, introduced to alleviate known limitations of classical semi-empirical roll damping estimation under large amplitude conditions. Particular emphasis was placed on improving amplitude dependency and nonlinear viscous contributions, which are known to govern the saturation stage of parametric rolling. The modular separation between excitation/restoring mechanisms and viscous dissipation allowed direct evaluation of how damping modelling influences the predicted instability envelope.

In addition to the reduced order model, high fidelity CFD simulations were performed to provide detailed insight into viscous flow phenomena, including bilge vortex formation, flow separation, and energy dissipation mechanisms that cannot be fully captured by semi-empirical approaches. Due to the substantial computational cost associated with fully nonlinear free surface CFD simulations involving large rigid body motions and overset mesh techniques, the comparison with experimental data was limited to a single representative condition. The comparison with experimental data is intended as an assessment of model performance rather than a formal validation in the strict verification and validation sense.

The case study is based on the well-documented APL China container vessel, which represents one of the first extensively reported full-scale incidents of parametric rolling. This ship has since become a benchmark case in both experimental and numerical investigations of parametric instability, providing a reliable reference for comparison purposes. The selected wave condition corresponds to a known resonance scenario, where the encounter frequency approaches twice the natural roll frequency, promoting the development of parametric rolling. This condition has been widely studied in previous numerical and experimental work. The choice of this specific case is therefore not arbitrary but is motivated by its relevance as a representative and well-established benchmark. Furthermore, the selected condition serves as a reference point for a broader parametric investigation, where additional wave lengths and heights are considered in subsequent analyses to assess the sensitivity of the rolling response.

To evaluate the predictive capability of the proposed methodology, assessment of model performance must be conducted under conditions where parametric rolling is known to occur. Benchmark cases for the C11-class container vessel (L_{pp} = 262.00 m, D = 24.40 m, B_{DWL} = 40.00 m, Δ_{DWL} = 76056 t and T_{DWL} = 12.34 m) have been documented by France et al. [3], with successful numerical reproduction reported by Belenky et al. [35] for a representative head sea condition (10 knots, 8.4 m wave height, 0.44 rad/s). Although instability in head waves has been observed within a broader speed range of approximately 7–11 knots, the present assessment is performed at 8 knots in regular head waves, ensuring operation within the established instability regime while maintaining consistency with the available experimental data. Accordingly, the present comparative analysis focuses exclusively on Test No. 9 conducted at CEHIPAR basin during HYDRALAB III project, corresponding to regular head waves with wave period T_W =12.95s, forward speed V = 8 kn, and wave height H_W = 8m as seen in Figures 9 and 10.

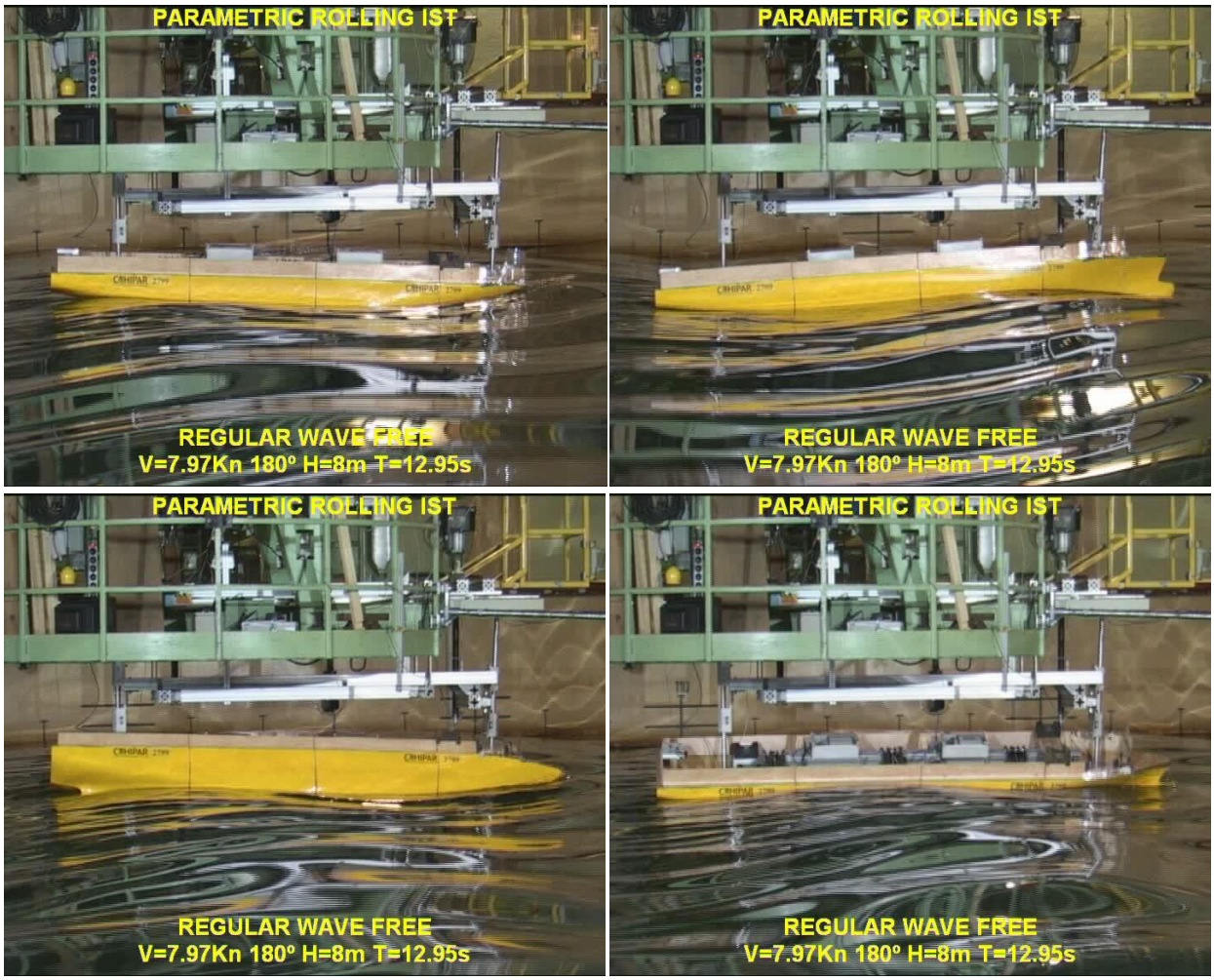

Fig. 9 Experimental footage of parametric rolling with regular head waves (H_W = 8 m, T_W = 12.95 s, speed 8 knots)

This condition corresponds to a wavelength-to-ship-length ratio of λ/Lpp = 1, where λ denotes the incident wavelength and *Lpp* the ship length between perpendiculars. This ratio represents the classical resonance regime for parametric rolling of container vessels. This wave-length-to-ship-length ratio is known to maximize the variation of the transverse metacentric height and thus create the strongest parametric excitation.

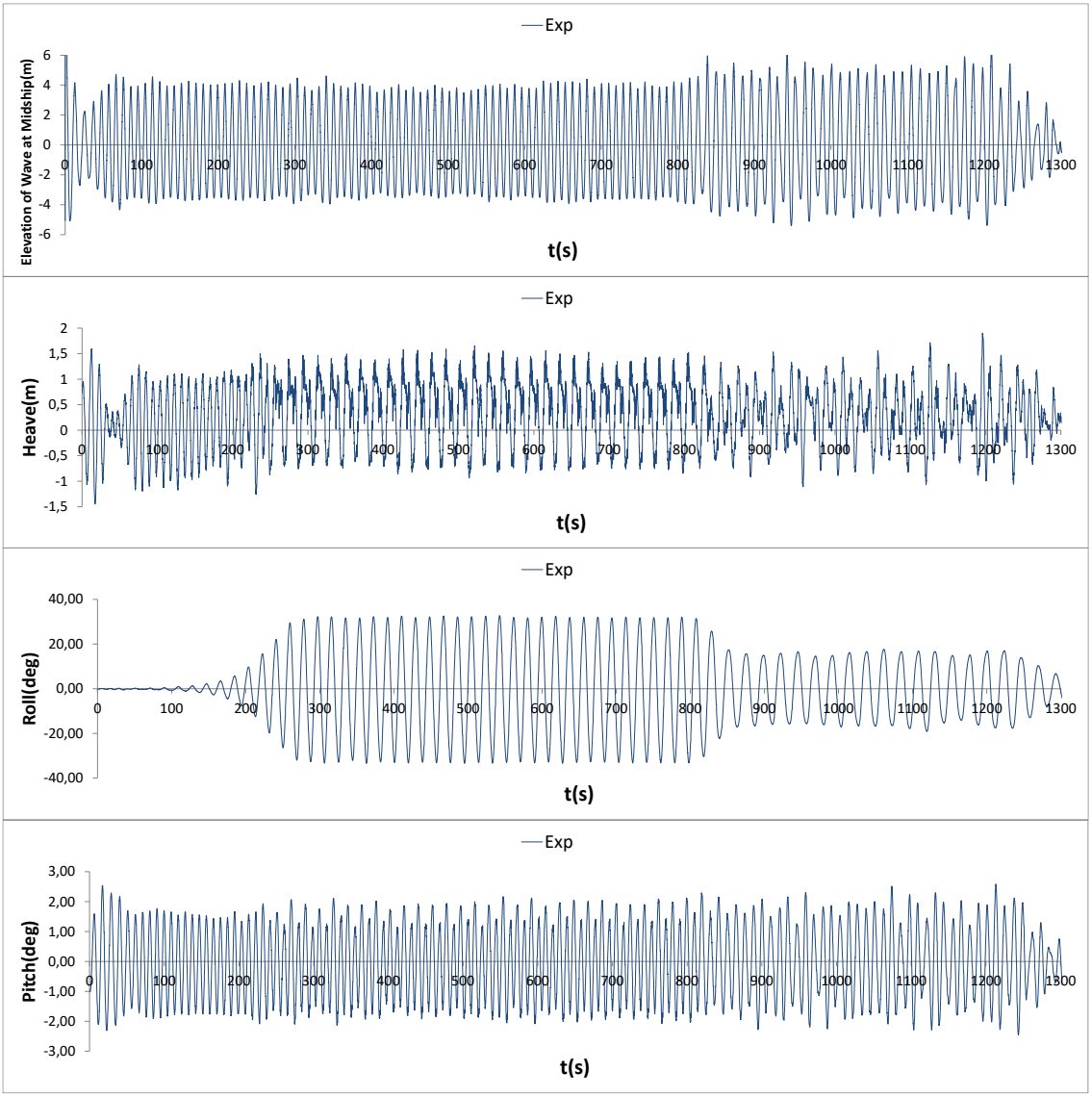

Fig. 10 Experimental development of parametric rolling with regular head waves (H_W = 8 m, T_W = 12.95 s, speed 8 knots)

The results are organized as follows. First, the nonlinear time domain predictions are examined, highlighting instability onset and amplitude growth characteristics and the influence of the blended Ikeda-based damping formulation on saturation levels. Finally, CFD simulations are introduced to assess the physical consistency of the viscous modelling assumptions and to quantify the differences arising from mesh motion strategies and numerical dissipation effects.

This structured comparison allows a systematic evaluation of the capability of the reduced order nonlinear model to reproduce experimentally observed instability, the sensitivity of roll amplitude to viscous damping representation, and the added value of CFD in resolving complex nonlinear flow mechanisms governing the ultimate roll response.

The nonlinear time domain model (Figure 11) was first implemented under the selected regular head wave condition. The computed heave and pitch responses exhibit nearly harmonic oscillations at the encounter frequency, confirming consistent excitation and restoring variation. In contrast, the roll response shows the characteristic behaviour of parametric instability, with gradual amplitude growth followed by saturation. The roll period is approximately twice the pitch period, consistent with the first parametric resonance condition. The results demonstrate that the numerical model correctly captures the fundamental mechanism of parametric rolling prior to experimental and CFD comparison.

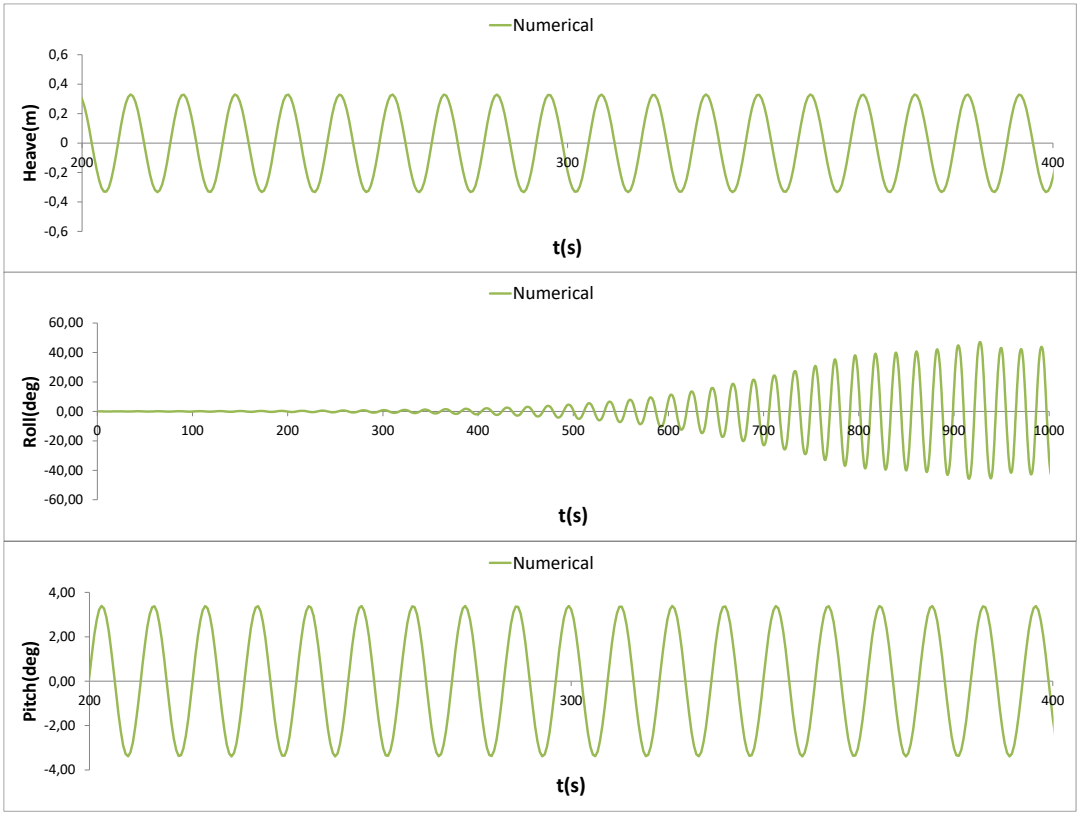

Fig. 11 Numerical development of parametric rolling with regular head waves (H_W = 8 m, T_W = 12.95 s, speed 8 knots)

The CFD simulation using the single-mesh approach (with direct mesh movement) was performed under the same regular head wave condition as seen in Figure 12.

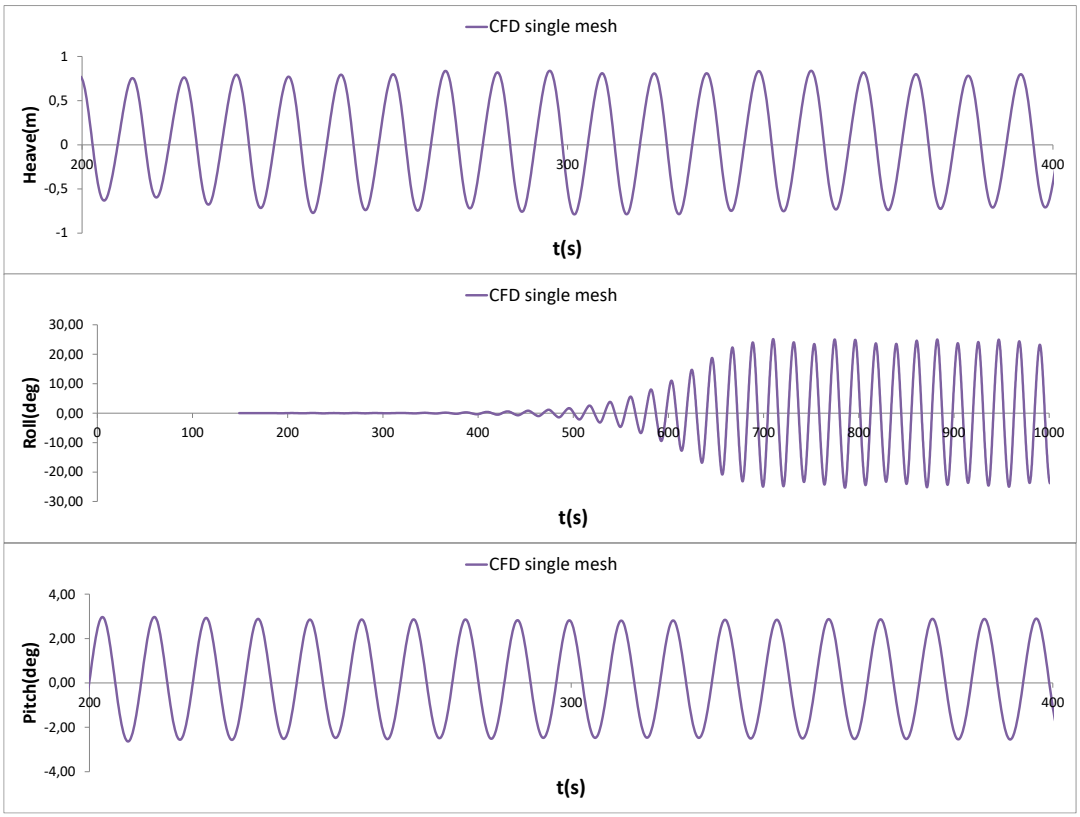

Fig. 12 CFD single-mesh approach development of parametric rolling with regular head waves (H_W = 8 m, T_W = 12.95 s, speed 8 knots)

The heave and pitch responses remain predominantly harmonic and follow the imposed encounter frequency, confirming consistent representation of the wave excitation. The roll response exhibits clear parametric amplification, with gradual exponential growth followed by saturation at approximately 25°. The overall behaviour reflects the characteristic features of first order parametric instability, including the roll period being approximately twice the pitch period.

The CFD simulation employing the overset mesh technique (Figure 13) was performed under the same regular head wave condition highlighting the same pattern as observed in the experiment (Figure 9) which depicts heave, roll and pitch motions.

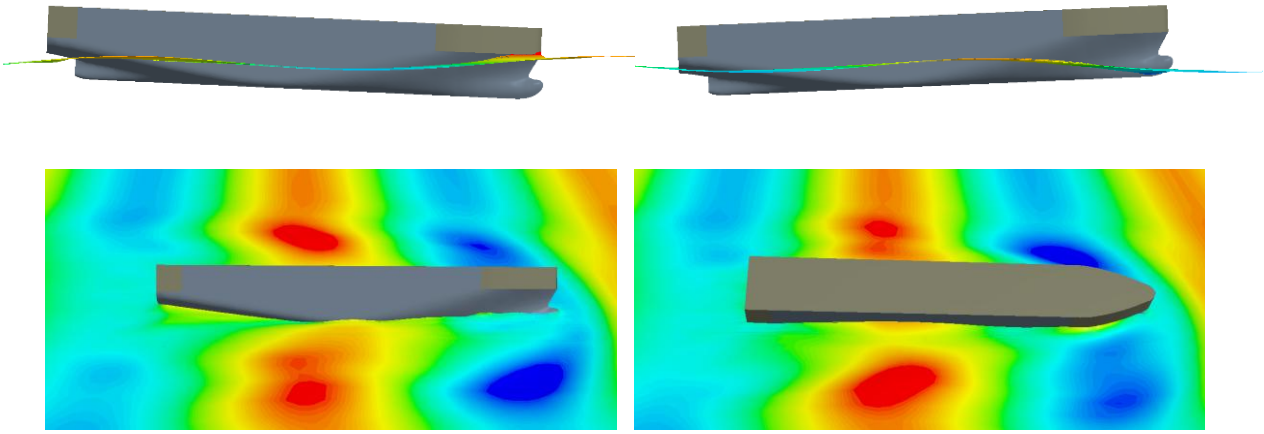

Fig. 13 CFD parametric rolling motion of the C11 vessel in head seas

The heave and pitch responses remain nearly harmonic and consistent with the imposed encounter frequency until the onset of parametric rolling. The roll response exhibits pronounced parametric amplification, with rapid exponential growth followed by saturation at amplitudes exceeding 40° as seen in Figure 14.

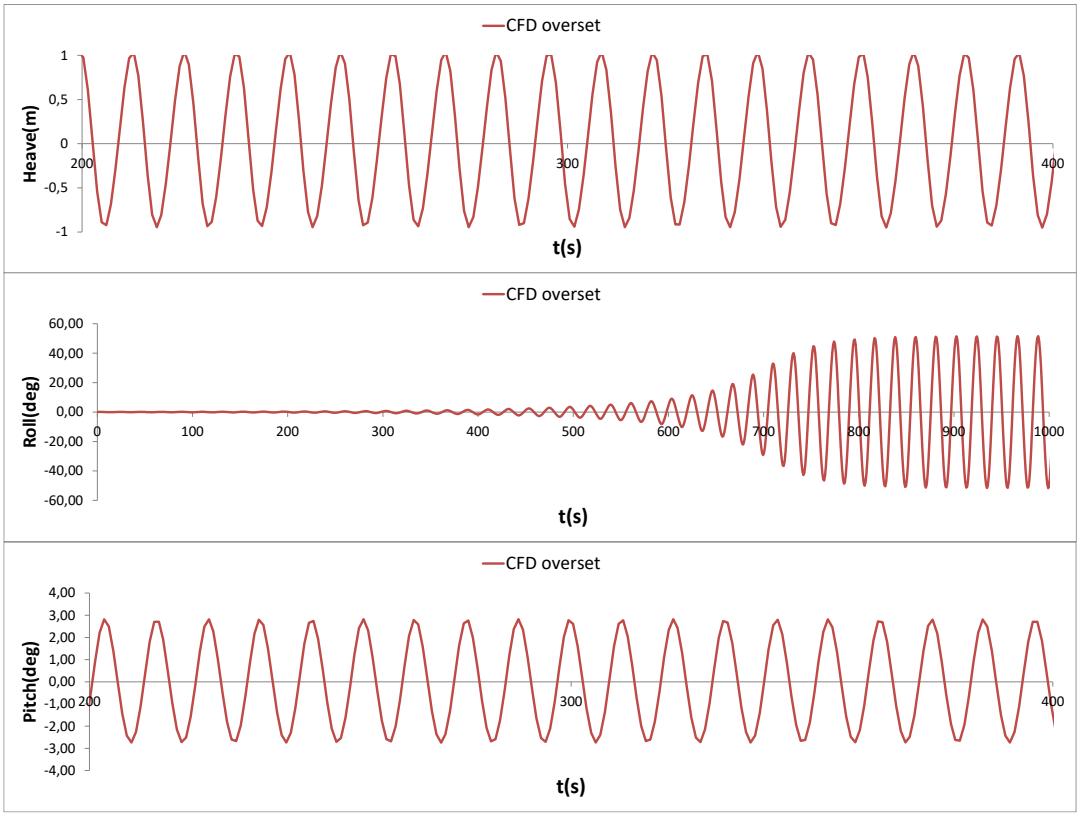

Fig. 14 CFD overset (chimera) grid technique development of parametric rolling with regular head waves (H_W = 8 m, T_W = 12.95 s, speed 8 knots)

The instability develops smoothly without numerical distortion, and the roll period remains approximately twice the pitch period, confirming preservation of the fundamental parametric resonance mechanism. The larger steady-state amplitude indicates reduced numerical dissipation and enhanced resolution of viscous flow effects during large roll motions.

The instability is triggered by unavoidable numerical perturbations arising from discretization and mesh asymmetry, which act as infinitesimal disturbances in the inherently unstable Mathieu system. The Figure 15 illustrates the asymmetric deformation of the free surface around the hull at large roll angles, as the ship rolls, highlighting the nonlinear wave–body interaction and the shift in local waterline elevation induced by parametric rolling.

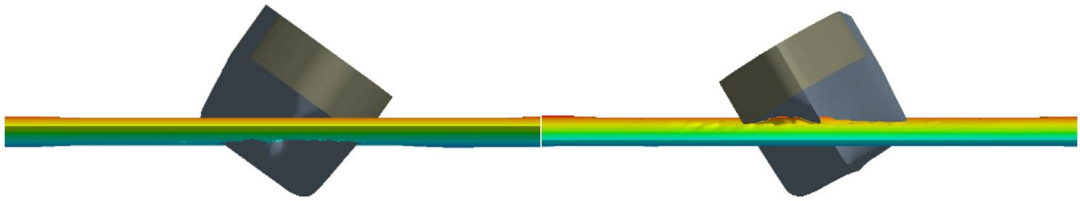

Fig. 15 Instantaneous free surface deformation during large amplitude roll motion

From a wave mechanics perspective, while the CFD simulations employ an ideal monochromatic wave corresponding to the nominal test specification, an experimental basin record reflects the actual free surface elevation experienced by the model. Therefore, they include small deviations in frequency and crest–trough asymmetry introduced by wave generation and basin effects. For the purpose of motion analysis within this work's context, the midship probe measurement provides the most representative description of the wave excitation acting on the vessel. The comparison of the measured midship wave elevation and the numerically imposed regular wave in Figure 16 reveals such a difference in dominant period and waveform shape.

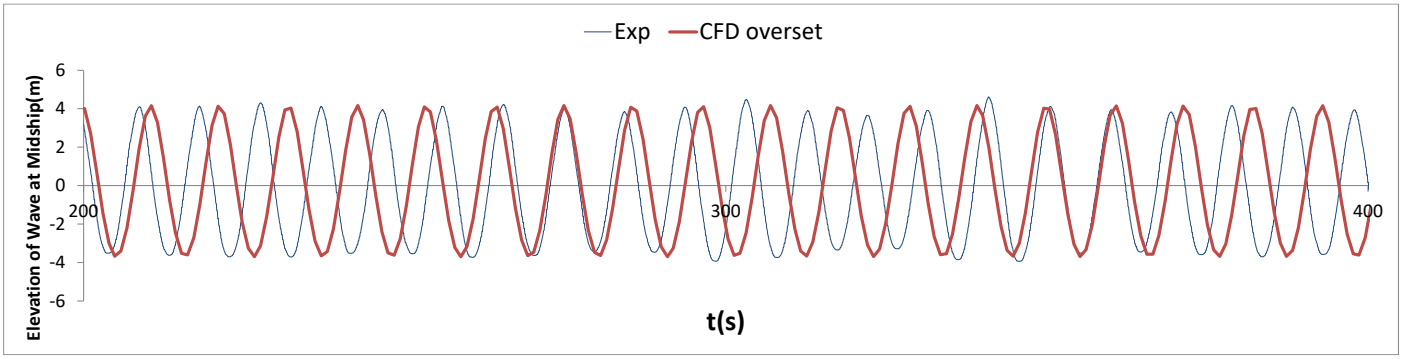

Fig. 16 Measured midship wave elevation and the numerically imposed regular

In theory, regular head waves were prescribed with (H_W = 8 m, T_W = 12.95 s), whereas in the basin, the measured wave probe signal is rarely a perfect sinusoid at exactly that single frequency, as mentioned. Accordingly, the experimental wave record in Figure 16 shows noticeable deviations from a pure regular wave (amplitude and shape variations), i.e., it contains additional frequency content beyond the target component. Even when the wavemaker was set to T_W =12.95 s, what matters for the ship response is the dominant component that actually reaches the model at the ship location (plus reflections, 2nd-order bound harmonics, and any slight wavemaker detuning). The numerical and CFD models were forced with the nominal regular wave period associated with Test No. 9. As stated in the experiments, the recorded wave elevation signal deviates from a perfect monochromatic wave and exhibits a slightly different dominant frequency at the model location. As a result, the effective encounter frequency differs slightly between experiment and simulations, leading to the observed differences in pitch and roll periods as seen from Figure 17. Because pitch response follows the encounter frequency and parametric roll develops at approximately twice that frequency, the observed shift in pitch and roll periods between experiment and simulations is consistent with this measured wave discrepancy.

With forward speed V, the ship "sees" an encounter frequency in head seas as:

$$\omega_e=\omega+kV \tag{12}$$

So even if the generated wave frequency ω were perfect, the encounter period $Te=2\pi/\omega_e$ depends on both ω and V. Small differences in the actual wave component (or in the effective speed in the test) shift T_e.

It is very well established that parametric roll occurs when the restoring variation is near twice roll frequency:

$$\omega_e \approx 2\omega_\phi \tag{13}$$

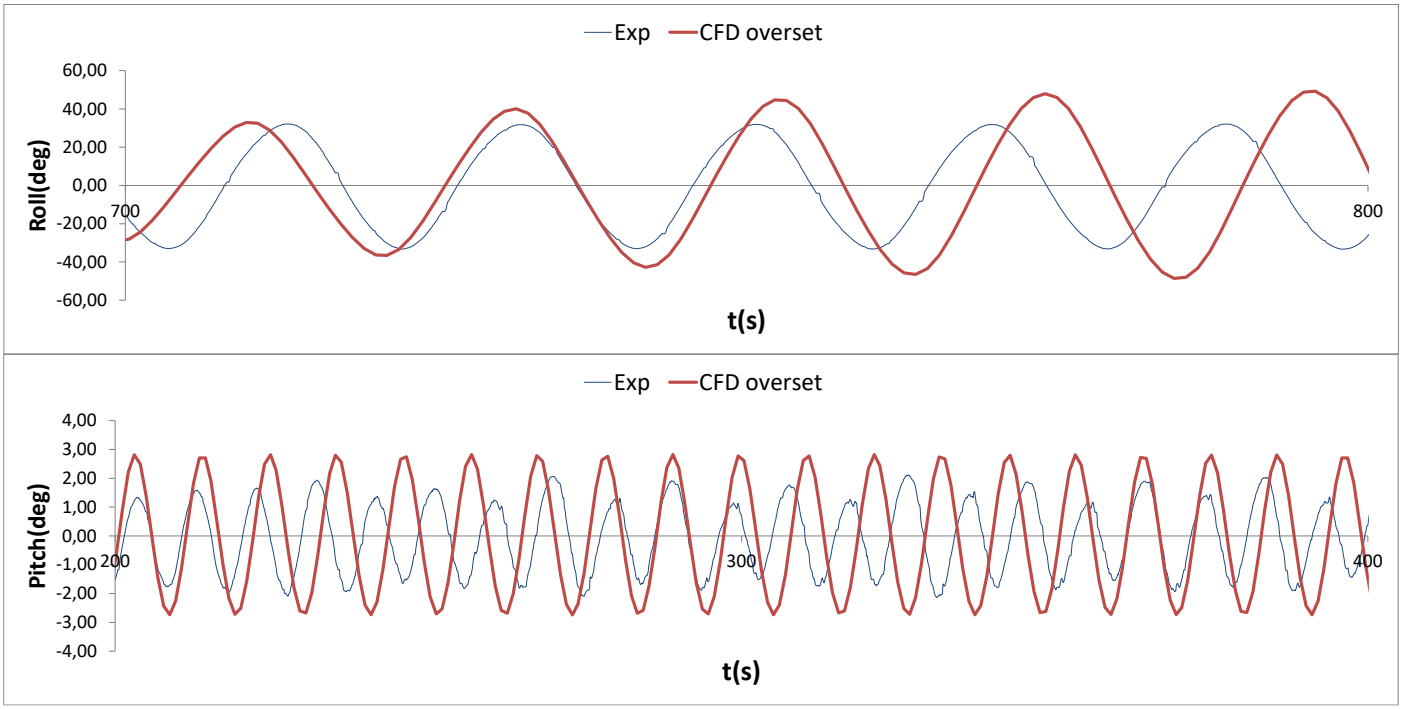

Fig. 17 Roll and pitch differences in periods for experiment CFD overset grid technique development of parametric rolling

That implies that pitch period in experiment ($T_{\text{pitch}} \approx 10$ s) for head seas is typically dominated by the encounter frequency and is close to it, while roll period is around $2T_{\text{pitch}} \approx 19$ s as seen from Figure 17. Looking at the window shown in plots (about 100 or 200 s), the experiment exactly shows that the parametric resonance signature (Mathieu type in Figure 18) and excitation/restoring varies at the encounter frequency, while roll responds at half of that frequency. So, the experiment is internally consistent, it's just cantered around a slightly higher frequency than numerical/CFD setup.

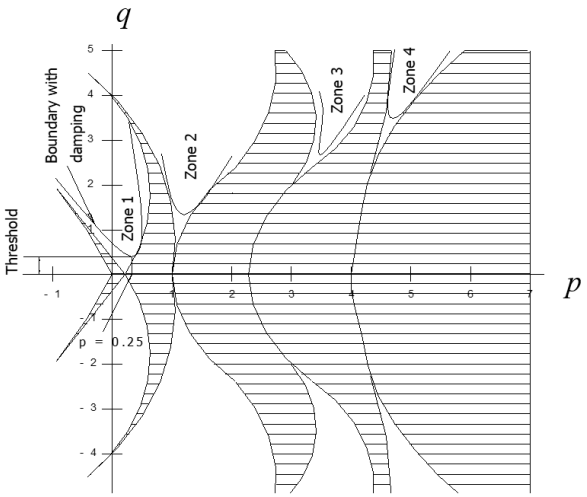

Fig. 18 Mathieu stability diagram

Both numerical/CFD show $T_{pitch} \approx 11.5$ s, and $T_{roll} \approx 22$ s, meaning the experiment has a slightly shorter effective encounter period than the "ideal" forcing used in CFD/time domain, so both pitch and roll will shift accordingly. The fact that experiment's "regular" wave contains a slightly different dominant period than the target even a modest shift in ω_e can move response closer to or farther from the "tongue" of instability and change both growth rate (how early it starts), response period and saturation level. Mathieu stability diagram shows shaded regions as instability "tongues" and white regions as stable solutions, where p represents normalized frequency parameter (that measures how close the 2:1 resonance condition is) and q modulation (excitation) amplitude parameter.

The first tongue (cantered near $p \approx 1$) is the classical parametric rolling condition and in this case the experiment and numerical values are at slightly different ω_e, that shifts the value of p horizontally. Keeping in mind that near the edges of the tongue, the solution is extremely sensitive to p, a small shift in ω_e can change growth rate, change onset time, and/or slightly change apparent roll period. If the experimental wave has a slightly shorter encounter period, that means slightly higher ω_e that shifts p and possibly moves the experiment deeper into the tongue. If it is deeper inside growth rate σ is larger, instability starts earlier, and amplitude grows faster, which is exactly what was observed.

Figure 19 presents the direct comparison of the nonlinear time domain solution (Numerical), CFD with single-mesh, and CFD with overset mesh under the selected head wave condition.

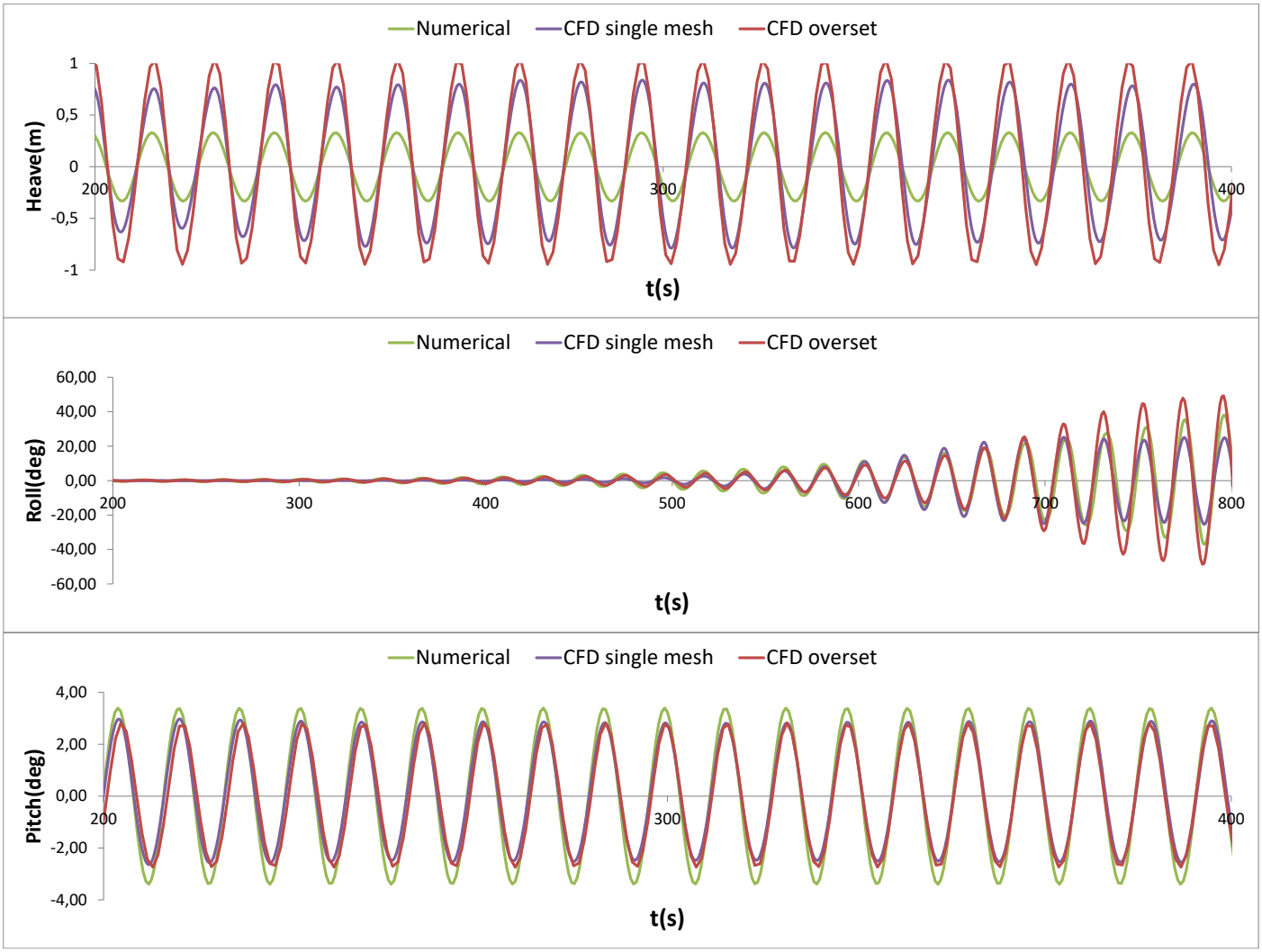

Fig. 19 Direct comparison of the nonlinear time domain solution (Numerical), CFD with single-mesh (CFD no overset) and CFD with overset mesh (CFD overset) for heave, roll and pitch responses

The responses in heave, roll, and pitch are shown over the same time interval to enable consistent assessment of amplitude and phase characteristics. The figure is intended to highlight consistency in dominant frequencies and to isolate amplitude differences arising from the modelling level and mesh motion strategy.

In heave, the dominant frequency is again consistent across all approaches; however, the numerical model predicts a noticeably lower amplitude, approximately half of the CFD response. This difference can be attributed to the reduced order nature of the time domain formulation, where the vertical excitation and hydrodynamic coupling are represented through simplified assumptions, while CFD resolves the fully nonlinear pressure field and free surface interaction, including local changes of wetted surface and nonlinear contributions to vertical force. Consequently, CFD tends to produce a stronger heave response in steep head waves.

The roll response exhibits the characteristic features of parametric instability in all three approaches: an initially small response followed by exponential amplification and subsequent saturation. The roll period remains approximately twice the pitch period, confirming that the fundamental resonance mechanism is preserved. A particularly important observation concerns this roll response. In all three approaches, the onset of parametric amplification occurs at nearly the same time instant. The exponential growth phase begins within a very narrow time window for the numerical model and both CFD configurations. This close agreement in instability onset demonstrates that the fundamental excitation/restoring interaction responsible for parametric resonance is consistently captured across modelling levels.

While the growth initiation is nearly identical, the saturation amplitudes differ. The primary discrepancy lies in the saturation amplitude. The overset CFD solution reaches the highest roll amplitudes, the non-overset CFD solution saturates at significantly lower levels, and the reduced order numerical prediction lies between the two. This behaviour is consistent with differences in effective dissipation as the single-mesh approach can introduce additional numerical damping due to grid distortion during large motions, while the overset strategy preserves mesh quality and tends to reduce artificial dissipation, allowing the instability to grow to larger amplitudes before nonlinear viscous effects balance the excitation.

The pitch responses show very close agreement in both frequency and amplitude across all three approaches, indicating that the imposed encounter conditions and the primary wave induced excitation in pitch are consistently reproduced. This agreement also suggests that the simplified excitation formulation in the time domain model is sufficient to capture the dominant pitch response for the present head wave case. Overall, the results confirm that the three approaches reproduce the same resonance condition and growth timing, while amplitude prediction remains sensitive to viscous modelling and mesh motion strategy.

Figure 20 reveals a key difference between the experimental measurements and all numerical predictions as the onset of parametric roll amplification in the experiment occurs significantly earlier than in the nonlinear time domain model and both CFD simulations. While the three numerical approaches exhibit very similar initiation times of exponential growth, the experimental response begins to amplify noticeably at an earlier stage.

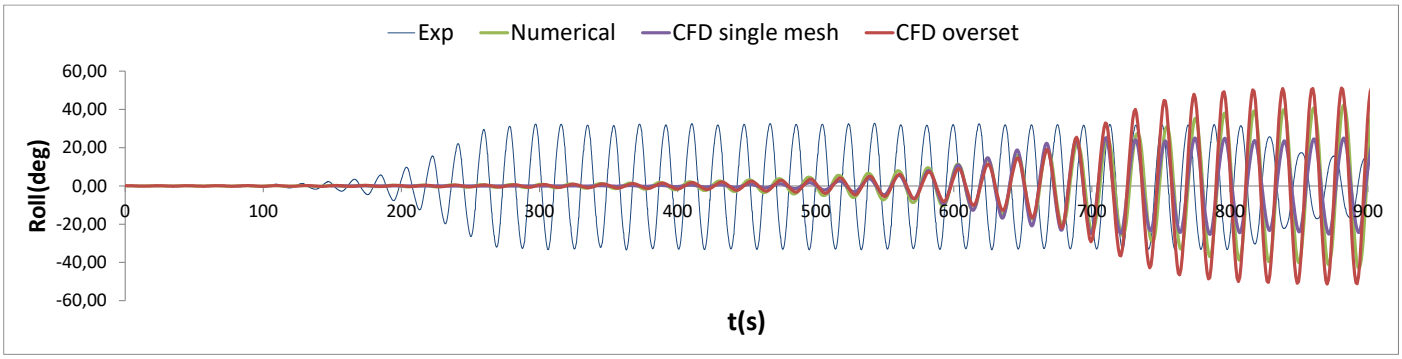

Fig. 20 Direct comparison of roll responses for experiment, the nonlinear time domain solution (Numerical), CFD with single-mesh (CFD no overset) and CFD with overset mesh (CFD overset)

This behaviour is consistent with the intrinsic nature of parametric instability. Parametric rolling corresponds to a Mathieu type instability figure, where the solution becomes unstable when the excitation frequency lies within the instability tongue. Once inside this region, the roll amplitude grows approximately exponentially,

$$\phi(t) \sim \phi_0 e^{\sigma t} \tag{14}$$

where the apparent onset time depends strongly on both the growth rate σ and, critically, on the initial perturbation amplitude ϕ_0.

In the towing tank experiment, the system is never perfectly symmetric or disturbance free. Unavoidable broadband perturbation, such as wave maker imperfections, small reflections from basin boundaries, carriage vibrations, minor geometric or mass asymmetries, and local free surface irregularities, provide a finite initial disturbance level. Because parametric resonance amplifies even infinitesimal perturbations, a slightly larger initial seed amplitude can lead to visibly earlier exponential growth. In contrast, all numerical approaches start from an almost perfectly symmetric and noise free state. The initial perturbation level is effectively limited to numerical roundoff and discretization errors. As a result, although the growth rate of the instability may be comparable, the smaller initial amplitude delays the moment at which exponential amplification becomes visually significant.

Importantly, once the instability develops, the three numerical solutions show very similar growth timing relative to one another, indicating that the excitation/restoring interaction and resonance condition are consistently captured. The discrepancy therefore lies not in the physical mechanism of parametric instability, but in the triggering conditions inherent to experimental versus numerical environments. This distinction is fundamental since the earlier experimental onset does not imply stronger excitation or modelling deficiency, but rather reflects the high sensitivity of parametric rolling to initial disturbances within the instability region.

While differences in the final roll amplitudes are observed between the experimental and numerical approaches, the primary objective of the present study is the correct reproduction of the instability mechanism rather than exact amplitude matching. Parametric rolling is fundamentally a resonance driven instability phenomenon. Therefore, capturing the correct excitation/restoring interaction, growth behaviour, and frequency relationship is of greater importance than reproducing a specific saturation amplitude.

Final aspect concluded from this research shows the CFD simulations exhibit a distinct modification of the heave response coinciding with the onset of roll amplification as seen in Figure 21. A transient shift of the mean heave level and waveform distortion are observed as roll amplitude increases similarly to experiment. This behaviour is attributed to nonlinear hydrostatic coupling and dynamic redistribution of energy between motion modes once large roll angles develop. The ability of the CFD model to reproduce this coupled response provides further evidence that the fundamental instability mechanism is correctly resolved.

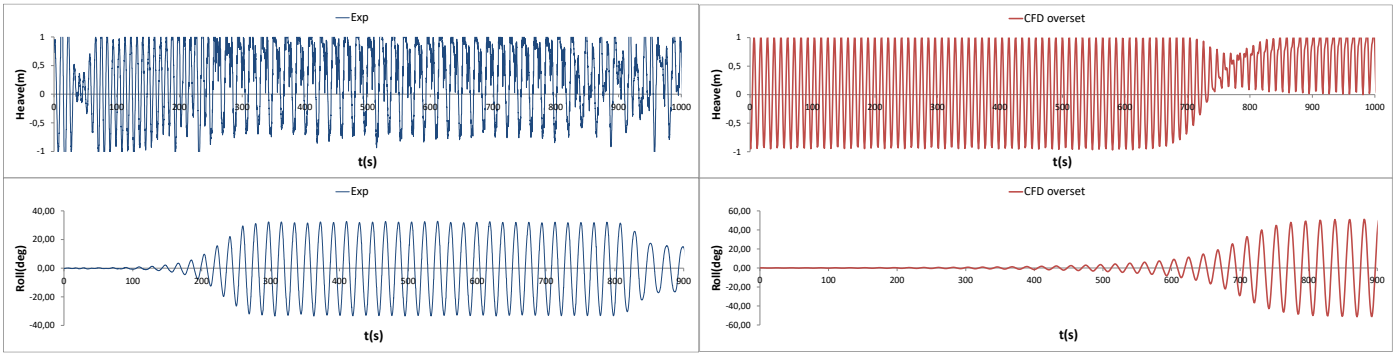

Fig. 21 Modification of the heave response coinciding with the onset of roll amplification for experiment and CFD overset

Parametric roll is not an isolated roll instability. The system equations contain nonlinear coupling terms in which roll affects vertical restoring, heave affects transverse stability and large roll activates second order cross terms. When roll energy increases rapidly energy is temporarily drawn from heave. This explains the distortion of the heave pattern and the transient amplitude modification. The absence of a corresponding heave mean shift in the numerical model indicates that the observed effect originates from strongly nonlinear

hydrostatic and hydrodynamic coupling mechanisms that are not represented within the potential flow-based formulation.

7. Discussion, Model Limitations, and directions for future work

While the present work provides valuable insight into the mechanisms governing parametric rolling and opens multiple directions for future investigation, it also highlights several limitations of the current modelling framework.

7.1 Influence of damping threshold on instability onset

One of the initial expectations of this study was that the fully viscous CFD simulations would predict earlier onset of parametric rolling compared to the potential flow based nonlinear time domain model. However, the results indicate that the onset of instability occurs within a very similar time window for all numerical approaches. This observation suggests that viscous damping has limited influence on the triggering condition once the system operates inside the instability region. According to classical stability analysis of the damped Mathieu equation, damping primarily shifts the instability boundaries rather than continuously modifying the onset behaviour. A critical damping threshold exists, above which the trivial solution remains stable and below which parametric resonance develops. Once the damping level falls below this threshold, the system behaves effectively in a binary manner: instability occurs, and the subsequent growth rate is determined by the balance between excitation and dissipation. The present results indicate that both the reduced order model and the CFD simulations operate below this critical damping level under the selected head wave condition. Consequently, the instability mechanism is activated in all cases at nearly the same time, while damping differences mainly influence saturation amplitude rather than initiation. A systematic parametric investigation of damping thresholds, both within the semi-empirical Ikeda framework and through controlled CFD variation of viscous effects would provide deeper insight into the stability boundaries and could clarify whether parametric rolling under realistic operational conditions indeed exhibits a near binary behaviour with respect to effective damping.

7.2 Influence of wave regularity and polychromatic forcing

Parametric rolling is classically studied under idealized monochromatic wave excitation. However, it is well known that severe parametric roll events in full scale conditions typically occur in sea states that are narrow banded and long crested, i.e., “almost regular” rather than fully irregular. The present experimental results indicate that the instability onset occurs earlier in the basin than in the idealized numerical simulations. This may be linked to the slight irregularity present in the measured wave record. Even small deviations from a purely monochromatic wave introduce additional frequency components and amplitude modulation effects. In the context of Mathieu type instability, such perturbations may temporarily shift the system deeper into the instability region or provide continuous excitation seeds that accelerate the exponential growth phase. Consequently, slight polychromaticity may enhance triggering without fundamentally altering the resonance mechanism. The availability of polychromatic wave experiments (already conducted) provides an opportunity to systematically investigate how spectral bandwidth influences instability onset, growth rate, and saturation amplitude. Such analysis would help bridge the gap between idealized regular wave theory and realistic ocean conditions and may clarify whether parametric rolling in nature requires narrowly banded seas or whether broader spectra can also sustain the instability.

7.3 Expansion of the validation matrix and statistical assessment

A further natural extension of this work is the systematic expansion of the comparison database and the inclusion of formal validation and uncertainty assessment. The reduced order numerical model has already been exercised over a large parameter space through thousands of simulations and has been previously well-supported against the fully numerical FREDYN framework [33]. This extensive numerical dataset enables identification of operating regions with elevated susceptibility to parametric rolling, as illustrated by stability and response maps obtained from large scale parameter sweeps.

In contrast, CFD simulations remain computationally expensive, particularly when free surface effects, large amplitude motions, and overset mesh techniques are employed. For this reason, CFD was used in the present study as a targeted high-fidelity tool and applied only to a limited number of representative cases. Building on the existing automated workflow for CFD case generation, a logical next step is to perform CFD simulations for a carefully selected subset of conditions extracted from the numerical database, specifically those cases that exhibit clear parametric excitation and span different levels of severity and proximity to the instability boundaries.

In parallel, additional experimental data are available and can be incorporated into the comparison matrix. Combining a broader set of experiments with a larger number of CFD benchmark cases would enable a more statistically meaningful assessment of model performance. Rather than evaluating agreement on a single case basis, future work should focus on distributions of key metrics (e.g., onset time, growth rate, and saturation amplitude), thereby improving robustness of conclusions and providing clearer guidance on uncertainty and applicability of each modelling level.

7.4 Quantitative instability growth analysis

Although the present study evaluates instability onset primarily through time-domain comparison, a more rigorous quantitative assessment of parametric growth could be achieved through envelope extraction using the Hilbert transform and subsequent logarithmic fitting of the exponential growth phase. Such an approach would allow direct estimation of the instability growth rate σ and enable objective comparison between experimental, reduced order, and CFD predictions. Given the large numerical database already available and the possibility of extending the CFD validation set, future work should focus on statistical evaluation of growth rates across multiple operating conditions. Mapping the dependence of σ on wave parameters, forward speed, and effective damping would provide deeper insight into the stability boundaries and allow direct comparison with theoretical Mathieu instability regions. This quantitative framework would further clarify the role of viscous dissipation and spectral characteristics of wave excitation in governing parametric roll development.

7.5 Green water effects and nonlinear deck interaction

The experimental results should not be interpreted as an absolute reference state independent of modelling assumptions. During the basin tests, additional strongly nonlinear phenomena were observed, including episodes of green water on deck during large roll cycles. Such events introduce additional energy dissipation, local impact loads, and potentially modified restoring characteristics due to transient deck immersion. These effects are not represented in the present CFD simulations and are beyond the scope of the reduced order numerical model. The time domain formulation is based on potential flow assumptions combined with semi-empirical damping and therefore cannot capture strongly nonlinear free surface phenomena such as water on deck impact, deck edge immersion, or transient flow separation associated with green water events. In the CFD setup, the geometry and computational domain were defined such that wave overtopping onto the deck was intentionally excluded in order to isolate the pure parametric resonance mechanism. While this approach ensures controlled comparison between models, it omits an important nonlinear dissipation mechanism observed experimentally. Consequently, differences in saturation amplitude should be interpreted in light of these modelling limitations. The consistent prediction of instability onset, exponential growth behaviour, and frequency characteristics across all approaches demonstrates that the fundamental parametric resonance mechanism is correctly captured. However, accurate prediction of extreme amplitudes under severe conditions may require explicit resolution of green water effects and strongly nonlinear deck flow interaction. Future CFD investigations will therefore incorporate modified geometry and extended free surface treatment to allow wave overtopping and direct modelling of bow green water events observed in the experiments.

7.6 Coupled parametric rolling and self-propulsion effects

An important and largely unexplored extension of the present work concerns the coupling between parametric rolling and self-propulsion dynamics. While parametric instability has been extensively studied under prescribed forward speed conditions, the interaction between large amplitude roll motion and propeller–

hull hydrodynamics remains insufficiently investigated. During severe parametric rolling, periodic variations in propeller immersion, asymmetric inflow, and thrust fluctuations may introduce feedback mechanisms affecting forward speed and encounter frequency. Since the resonance condition is directly dependent on encounter frequency, such coupling may alter instability growth characteristics and saturation behaviour. Integration of the present parametric rolling framework with advanced self-propulsion CFD modelling offers a promising direction for future research and may provide new insights into nonlinear ship, propulsion and wave interaction under extreme operating conditions.

8. Conclusions

Parametric rolling of a container vessel in regular head waves was investigated using a hierarchical modelling framework combining a nonlinear time domain solver, a blended Ikeda based damping module, and CFD simulations employing both single-mesh and overset mesh strategies. The selected case (λ/Lpp = 1, H_W = 8 m, V = 8 kn) corresponds to a classical resonance condition known to trigger parametric instability.

All numerical approaches consistently reproduced the fundamental mechanism of parametric rolling, including the characteristic frequency relationship between pitch and roll motions and the exponential growth phase preceding saturation. A key result is the close agreement in the predicted instability onset between the reduced order model and both CFD configurations. Notably, the CFD simulations developed parametric rolling without any imposed initial heel, asymmetry, or artificial numerical perturbation, indicating that the instability emerged naturally from the interaction between the incident wave field and the ship restoring characteristics.

The experimental results showed an earlier onset of roll amplification, which is attributed to unavoidable perturbations and slight irregularities in the basin generated wave record. Differences in the predicted saturation amplitude are primarily related to viscous dissipation modelling and additional nonlinear phenomena observed in the experiment, such as green water on deck. These effects were not included in the present CFD configuration and cannot be represented within the potential based time domain model.

Overall, the study demonstrates that the fundamental instability mechanism of parametric rolling can be robustly captured across modelling levels, from reduced order numerical models to high fidelity CFD. Accurate prediction of the final roll amplitude, however, remains sensitive to nonlinear damping mechanisms and strongly nonlinear free surface effects. The developed framework provides a solid basis for future investigations addressing damping thresholds, irregular wave excitation, green water effects, and the coupling between parametric rolling and self-propulsion. The main finding of this study is that high-fidelity CFD simulations can reproduce parametric rolling purely from the governing physics, without artificial excitation or imposed asymmetry, while demonstrating that the choice of numerical setup, particularly mesh strategy and boundary treatment has a direct impact on the predicted roll response.

ACKNOWLEDGMENTS

This work was supported by the Croatian Science Foundation under the project project IP-IP-2022-10-2821 and by the University of Rijeka (PROJECTS no. PU-17 uniri-iz-25-10 - Funded by the European Union – NextGenerationEU).

REFERENCES

[1] Ribeiro E Silva, S., Turk, A., Guedes Soares, C., Prpić-Oršić J. 2010. On the parametric rolling of container vessels. *Brodogradnja*, 61(4), 347-358.

[2] Turk, A. 2012. Coupled nonlinear parametric resonance model for container ships. *Doctoral thesis*.

[3] France, W. N., Levandou, U. M., Treakle, T. W., Paulling, J. R., Michel, R. K., Moore, E. C., 2003. An Investigation of Head-Sea Parametric Rolling and its Influence on Container Lashing Systems. *Marine Technology* 40(1), 1-19. https://doi.org/10.5957/mt1.2003.40.1.1

[4] Kianejad, S. S., Enshaei, H., Duffy, J., Ansarifard, N., Ranmuthugala, D. 2019. Ship roll damping coefficient prediction using CFD. *Journal of Ship Research*, 63(02), 108-122. https://doi.org/10.5957/JOSR.07220021

[5] Sadat-Hosseini, H., Stern, F., Olivieri, A., Campana, E.F., Hashimoto, H., Umeda, N., Bulian, G., Francescutto, A. 2010. Head-wave parametric rolling of a surface combatant. *Ocean Engineering*, 37(10), 859-878. https://doi.org/10.1016/j.oceaneng.2010.02.010

[6] Liu, L., Chen, M., Wang, X., Zhang, Z., Yu, J. Feng, D. 2021. CFD prediction of full-scale ship parametric roll in head wave. *Ocean Engineering*, 233, 109180. https://doi.org/10.1016/j.oceaneng.2021.109180

[7] Zhou, Y.-H., Ning, M., Jiang, L., Min, G. 2016. A study of hybrid prediction method for ship parametric rolling. *Journal of Hydrodynamics*, 28(4), 617-628. https://doi.org/10.1016/S1001-6058(16)60666-2

[8] Bilandi, R.N., Mancini, S., Dashtimanesh, A., Tavakoli, Sasan. 2024. A revisited verification and validation analysis for URANS simulation of planing hulls in calm water. *Ocean Engineering*, 293, 116589. https://doi.org/10.1016/j.oceaneng.2023.116589

[9] Liu L., Zhang B., Zhang H., Gong J., Tian Z., Guo S., Bao Y., Zheng X. 2024. Study on numerical simulation and mitigation of parametric rolling in a container ship under head waves. *Brodogradnja* 75(3), 75305. https://doi.org/10.21278/brod75305

[10] Yıldız, B., Şener, B., Yurtseven, A., Katayama, T. 2019. Numerical and experimental calculation of roll amplitude effect on roll damping. *Brodogradnja*, 70(2), 1-15. https://doi.org/10.21278/brod70201

[11] Wang, S., Wei, J., Chen, X., Liu, L., Zhang, Z., 2019. Numerical simulations of KCS parametric rolling in head waves. *International Conference on Offshore Mechanics and Arctic Engineering* (OMAE 2019), 9-14 June, Glasgow, Scotland, UK. https://doi.org/10.1115/OMAE2019-95563

[12] Zhang, W., Liu, Y.-D., Chen, C., He, Y.-P., Tang, Y.-Y., Sun, J.-J. 2023. Research on the parametric rolling of the KCS container ship. *Journal of Marine Science and Technology*, 28(3), 675-688. https://doi.org/10.1007/s00773-023-00948-3

[13] Liu, L., Chen, M., Wang, X., Zhang, Z., Yu, J., Feng, D. 2021. CFD prediction of full-scale ship parametric roll in head wave. *Ocean Engineering*, 233, 109180. https://doi.org/10.1016/j.oceaneng.2021.109180

[14] Marlantes, K., Bandyk, P., Maki, K. 2023. Investigating Nonlinear Forces in Ship Dynamics using Machine Learning, *10th Conference on Computational Methods in Marine Engineering* (Marine 2023), 27-29 June, Madrid, Spain. https://doi.org/10.23967/marine.2023.051

[15] Zhou, X., Li, H., Huang, Y., Liu, Y. 2023. Deep learning machine-based ship parametric rolling simulation and recognition algorithms. *Ocean Engineering*, 276, 114137. https://doi.org/10.1016/j.oceaneng.2023.114137

[16] Liu, L., Feng, D., Wang, X., Zhang, Z., Yu, J., Chen, M. 2022. Numerical study on the effect of sloshing on ship parametric roll. *Ocean Engineering*, 247, 110612. https://doi.org/10.1016/j.oceaneng.2022.110612

[17] Phuong, N. T. H., Taniguchi, T., Katayama, T. 2025. Numerical study of scale effects of viscous roll damping for a container ship. *Brodogradnja*, 76(4), 76406. https://doi.org/10.21278/brod76406

[18] Halder, P., Liu, S. 2025. Numerical investigation of added resistance of a container ship in short regular waves using unsteady RANS simulations. *Brodogradnja*, 76(2), 76204. https://doi.org/10.21278/brod76204

[19] Jia, G., Jiao, J., Chen, C., Wu, T. 2025. CFD simulation of wave-induced motions of an LNG ship considering tank sloshing effects. *Brodogradnja*, 76(3), 76307. https://doi.org/10.21278/brod76307

[20] Tavakoli, S., Singh, M., Hosseinzadeh, S., Hu Z., Shao, Y., Wang, S., et al. 2025. A review of flexible fluid-structure interactions in the ocean: Progress, challenges, and future directions. *Ocean Engineering*, 342(1). 122545. https://doi.org/10.1016/j.oceaneng.2025.122545

[21] Faltinsen, O. M. 1990. Sea Loads on Ships and Offshore Structures. *Cambridge University Press*. https://doi.org/10.1146/annurev.fl.22.010190.000343

[22] Journée, J. M. J., Massie, W. W. 2001. Offshore Hydromechanics. *Delft University of Technology*.

[23] Ikeda, Y., 2004. Prediction methods of roll damping of ships and their application to determine optimum stabilization devices. *Marine Technology*, 41(2), 89-93. https://doi.org/10.5957/mt1.2004.41.2.89

[24] ITTC, 2024. Practical Guidelines for Ship CFD Applications. *ITTC Recommended Procedures and Guidelines*, 7.5-03-02-03, Revision 02.

[25] Menter, F.R., 1999. Two-equation eddy-viscosity turbulence models for engineering applications. *Aerospace Science and Technology*, 4(5), 159-171. https://doi.org/10.2514/3.12149

[26] Muzaferija S., Perić M., 1997. Computation of free-surface flows using the finite-volume method and moving grids. *Numerical Heat Transfer*, 32(4), 369-84. https://doi.org/10.1080/10407799708915014

[27] Perić, R., Abdel-Maksoud, M. 2015. Generation of free-surface waves by localized source terms in the continuity equation. *Ocean Engineering*, 109, 567-579. https://doi.org/10.1016/j.oceaneng.2015.08.030

[28] Jiang, Z., Tavakoli, S., Kujala, P., Hirdaris, S. 2023.A two-dimensional Reynolds averaged Navier–Stokes investigation on gap resonance and wave elevation around two side-by-side bodies with motions. *Physics of Fluids*, 35, 127129. https://doi.org/10.1063/5.0180027

[29] Karola, A., Tavakoli, S., Mikkola, T., Matusiak, J., Hirdaris, S. 2024. The influence of wave modelling on the motions of floating bodies. *Ocean Engineering*, 306, 118067. https://doi.org/10.1016/j.oceaneng.2024.118067

[30] Mancini, S., Begovic, E., Day, A.H., Incecik A. 2018 Verification and validation of numerical modelling of DTMB 5415 roll decay. *Ocean Engineering,* 162, 209-223. https://doi.org/10.1016/j.oceaneng.2018.05.031

[31] Gokce, M. K., Kinaci, O. K. 2018. Numerical simulations of free roll decay of DTMB 5415. *Ocean Engineering*, 159, 539-551. https://doi.org/10.1016/j.oceaneng.2017.12.067

[32] Irkal, M.A.R., Nallayarasu, S., Bhattacharyya S.K. 2019. Numerical prediction of roll damping of ships with and without bilge keel. *Ocean Engineering*, 179, 226-245. https://doi.org/10.1016/j.oceaneng.2019.03.027

[33] Huang, L., Pena, B., Thomas, G. 2023. Towards a full-scale CFD guideline for simulating a ship advancing in open water. *Ship technology research*, 70, 222-238. https://www.tandfonline.com/doi/full/10.1080/09377255.2023.2167537#d1e148

[34] Gray-Stephens, A., Tezdogan, T., Day, A.J. 2021. Minimizing numerical ventilation in computational fluid dynamics simulations of high-speed planing hulls. *Journal of Offshore Mechanics and Arctic Engineering*, 143(3), 031903. https://doi.org/10.1115/1.4050085

[35] Belenky, V. L., Weems, K. M., Lin, W. M., Paulling, J. R., 2011. Probabilistic Analysis of Roll Parametric Resonance in Head Seas. *Fluid Mechanics and Its Applications*, 97, 555-569. https://doi.org/10.1007/978-94-007-1482-3_31